Electronic Supplementary Information (ESI)

Kinetically Labile Ruthenium(II) Complexes of Terpyridines and Saccharin: Effect of Substituents on Photoactivity, Solvation Kinetics, and Photocytotoxicity

Priyaranjan Kumar[a], Prerana Singh[b], Sanjoy Saren[a], Sandip Pakira[a], Sri Sivakumar[b], Ashis. K. Patra*[a]

Author address: [a]Department of Chemistry, Indian Institute of Technology Kanpur, Kanpur 208016, Uttar Pradesh, India.

[b]Department of Chemical Engineering, DST Thematic Unit of Excellence on Soft Nanofabrication, Indian Institute of Technology Kanpur, Kanpur 208016, Uttar Pradesh, India.

[c]Department of Biological Sciences & Bioengineering, Indian Institute of Technology Kanpur, Uttar Pradesh 208016, India

Contents Page

General characterizations

X-ray diffractions studies

Solvation and kinetics studies

Photoactivity

Biological studies

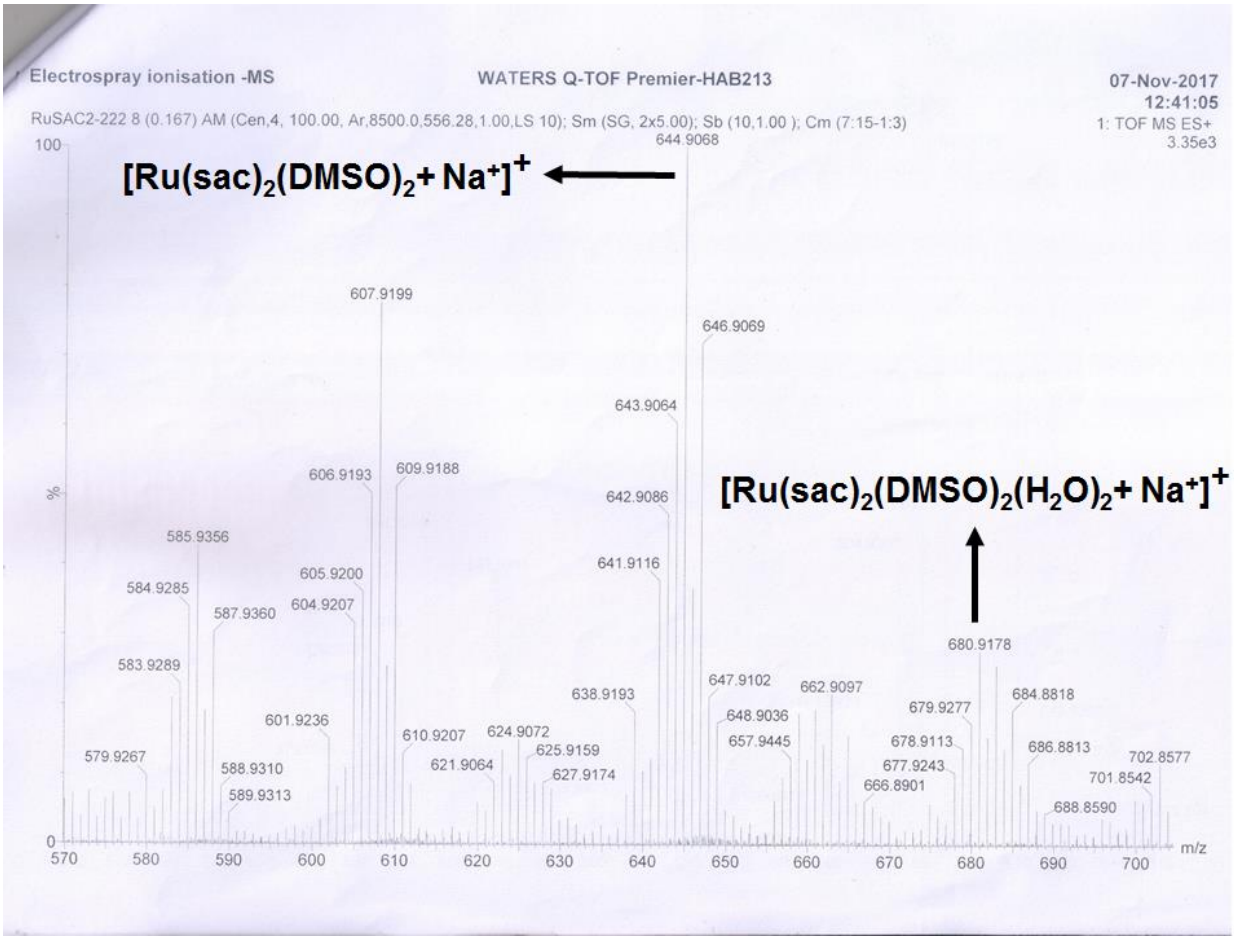

Fig. S1. ESI-MS(+) of complex *trans*-[Ru(sac)$_2$(H$_2$O)$_3$(dmso-*S*)] (**1**) in H$_2$O.

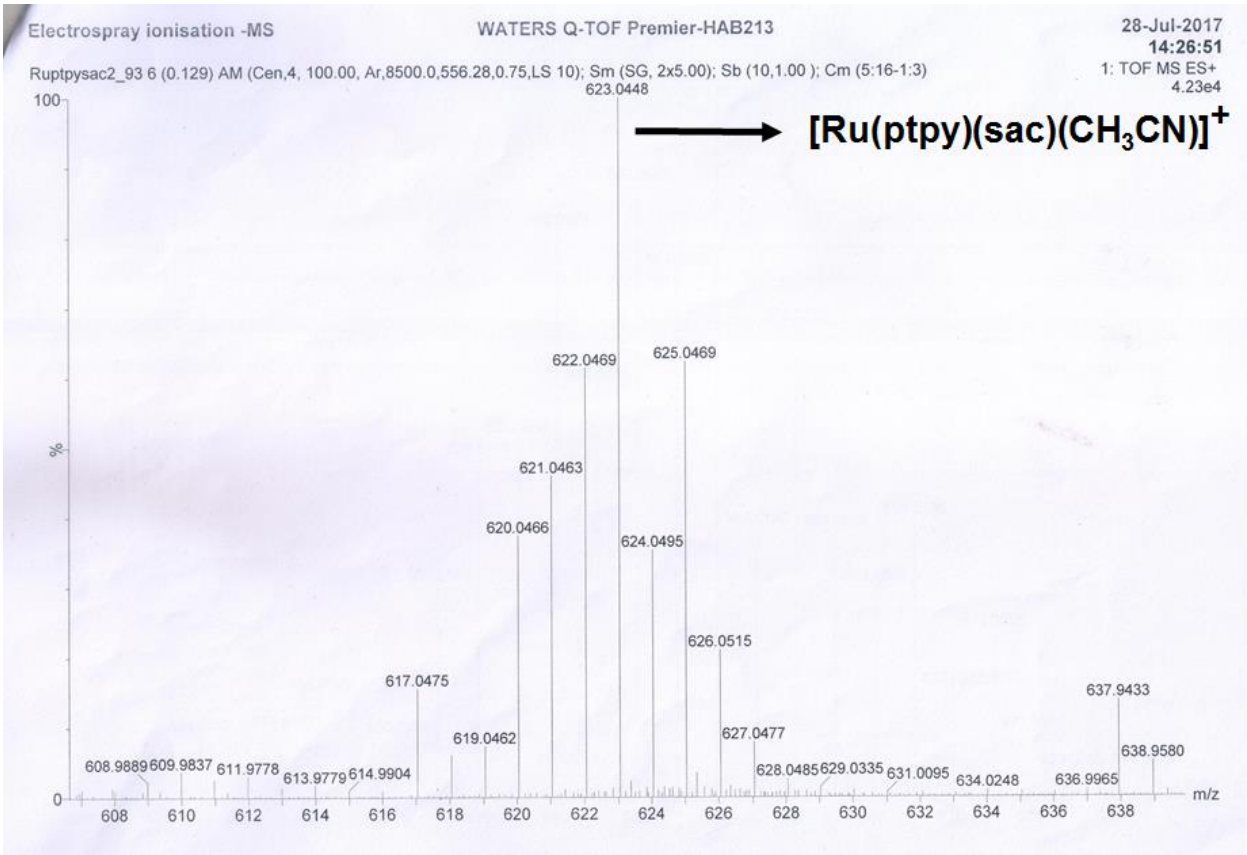

Fig. S2. ESI-MS(+) of complex [Ru(ptpy)(sac)$_2$(dmso)] (**2**) in CH_3CN.

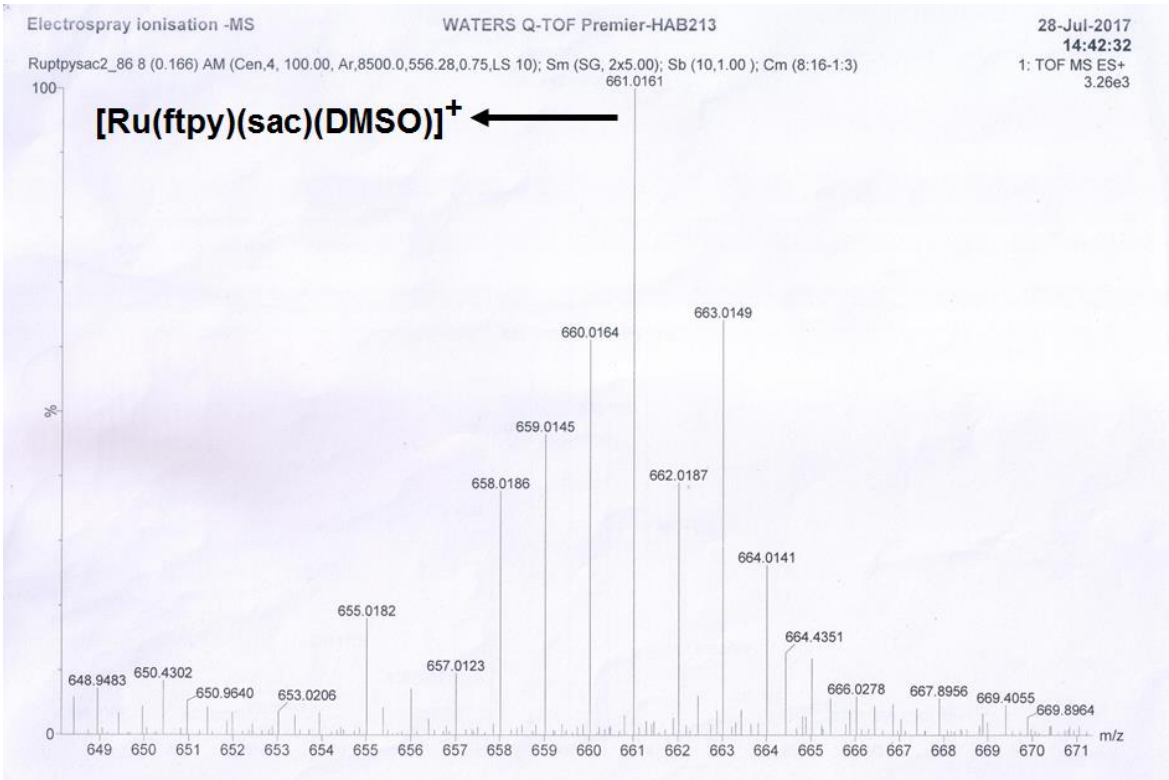

Fig. S3. ESI-MS(+) of [Ru(ftpy)(sac)$_2$(dmso)] (**3**) in methanol.

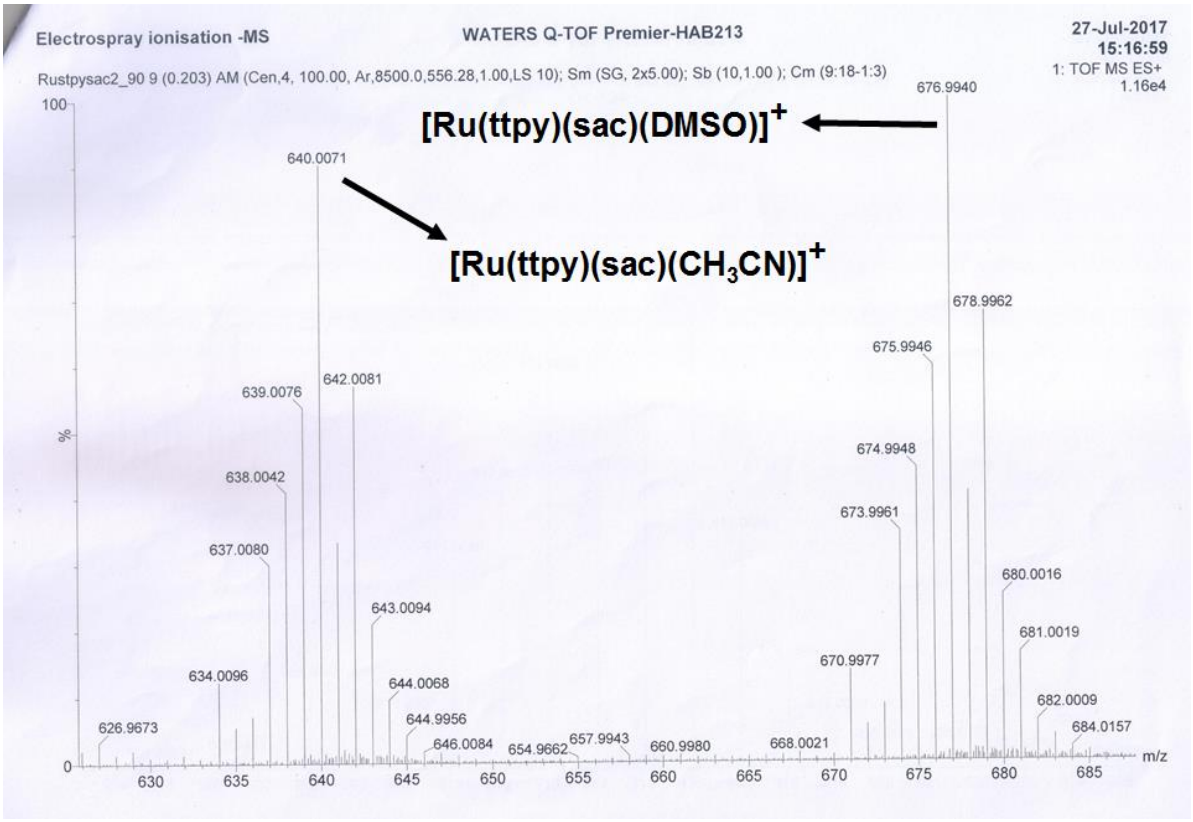

Fig. S4. ESI-MS(+) of [Ru(ttpy)(sac)$_2$(dmso)] (**4**) in CH_3CN.

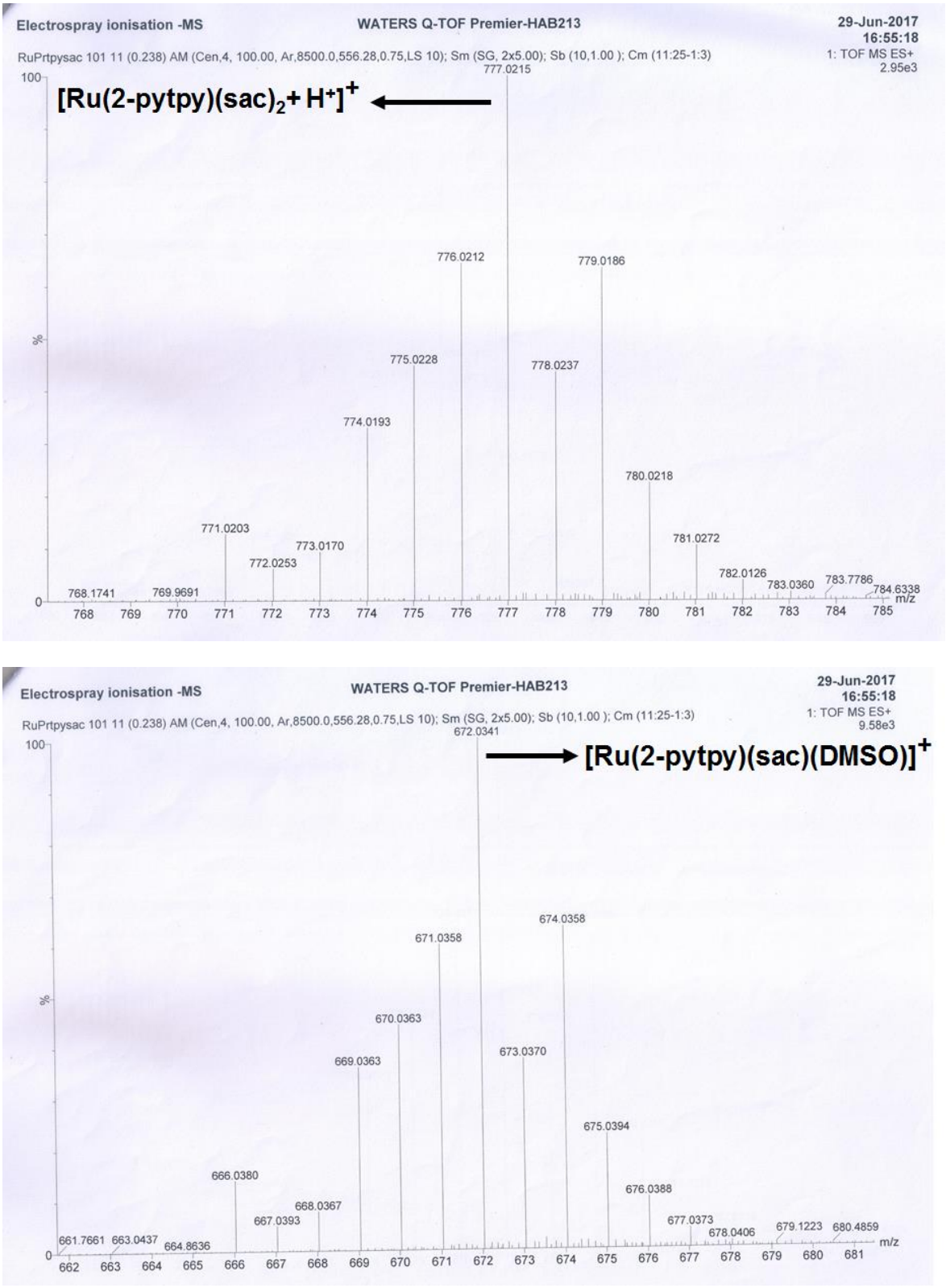

Fig. S5. ESI-MS(+) of complex [Ru(2-pytpy)(sac)$_2$(dmso)] (**5**)in methanol showing [M-(DMSO)+ H^+]$^+$ (top) and [M-(sac)$^-$]$^+$ (bottom).

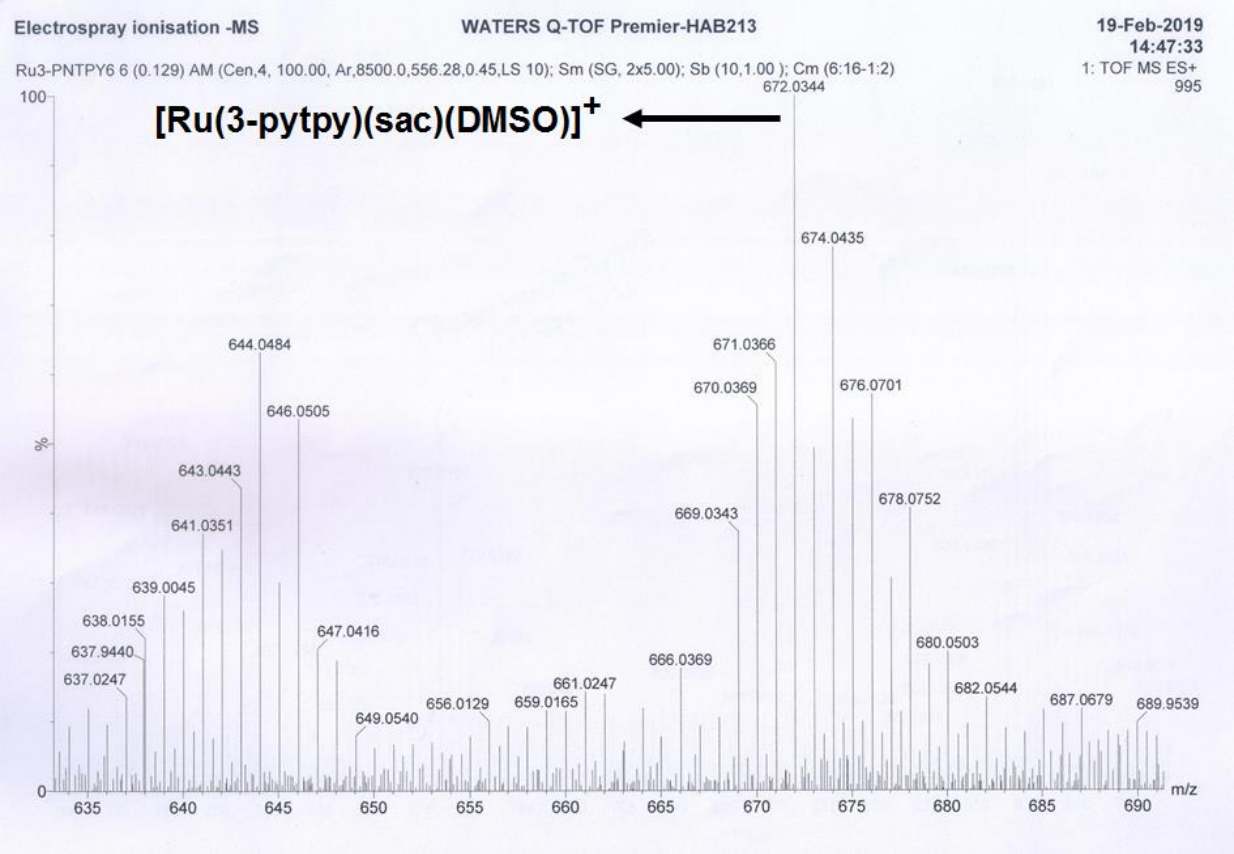

Fig. S6. ESI-MS(+) of complex[Ru(3-pytpy)$(sac)_2$(dmso)] (**6**) in methanol.

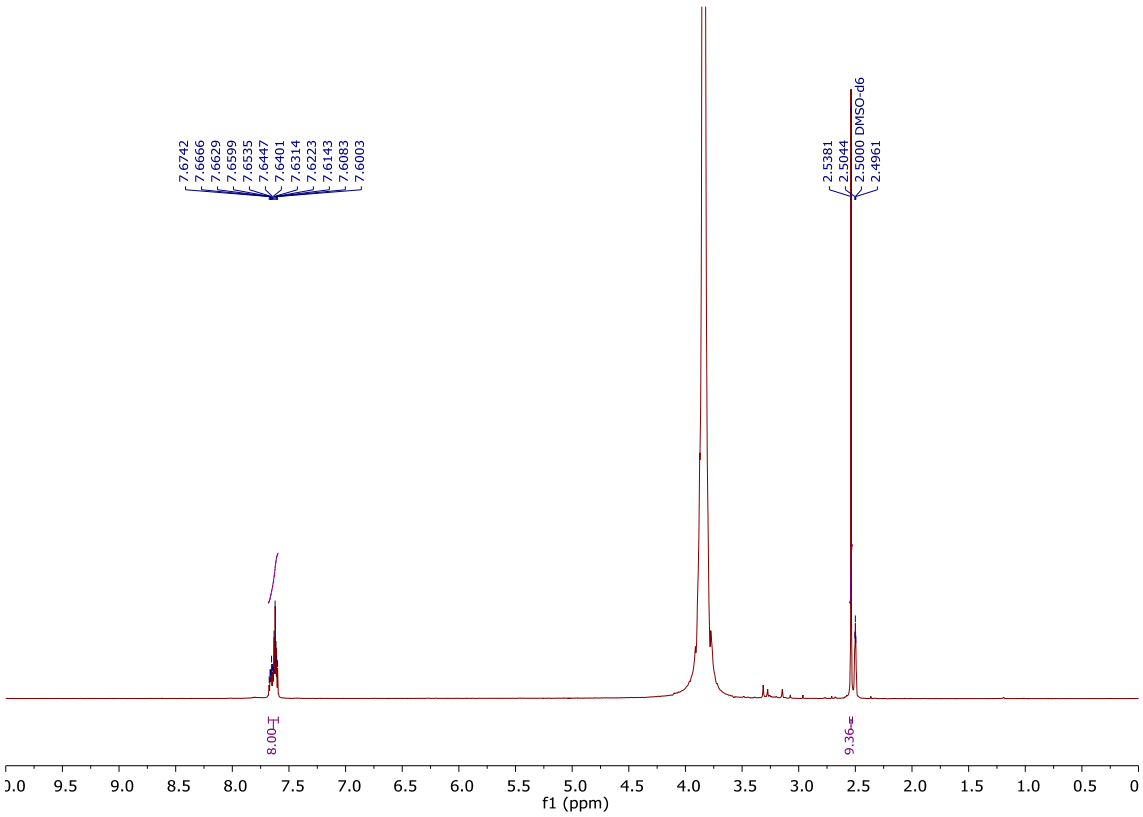

Fig. S7. ^{1}H-NMR spectra of complex **1** (400 MHz, DMSO-d_6) at 298 K.

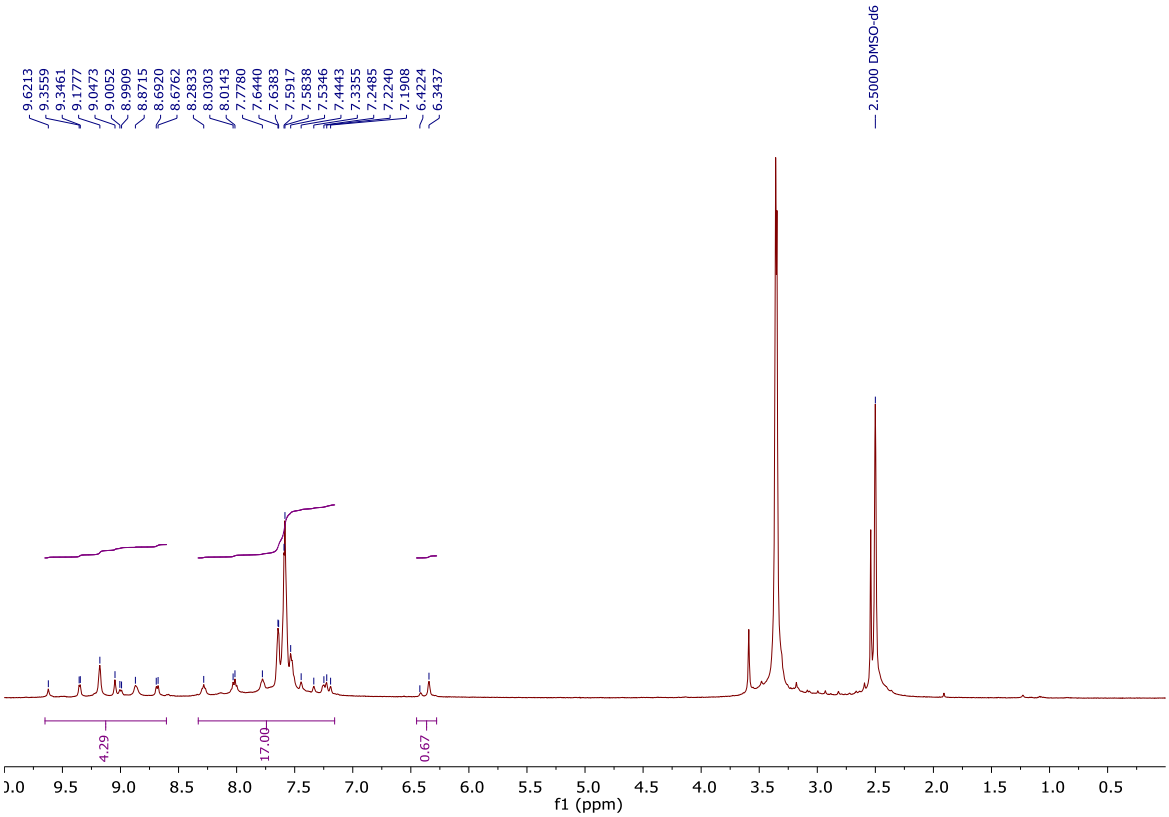

Fig. S8. ^{1}H-NMR spectra of complex **2** (500 MHz, DMSO-d_6) at 298 K.

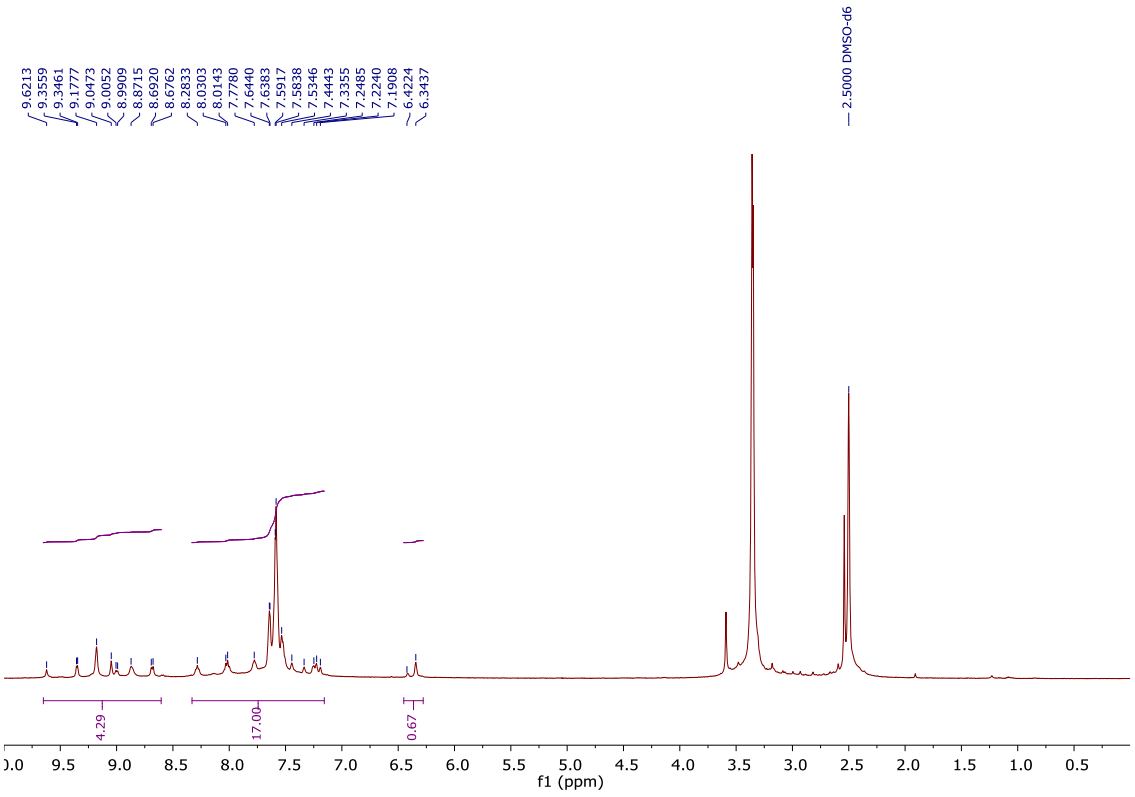

Fig. S9. ^{1}H-NMR spectra of complex **3** (500 MHz, DMSO-d_6) at 298 K.

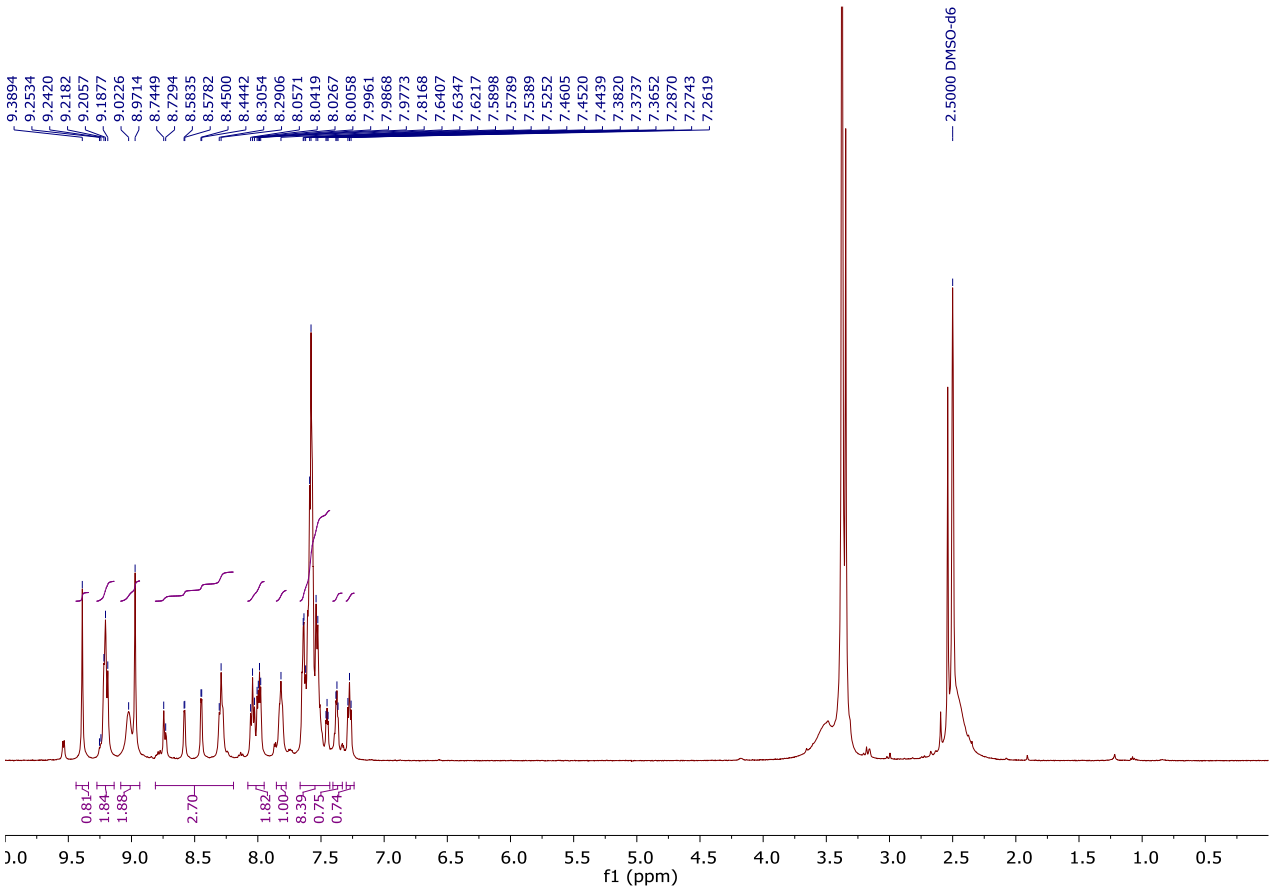

Fig. S10. ^{1}H-NMR spectra of complex **4** (500 MHz, DMSO-d_6) at 298 K.

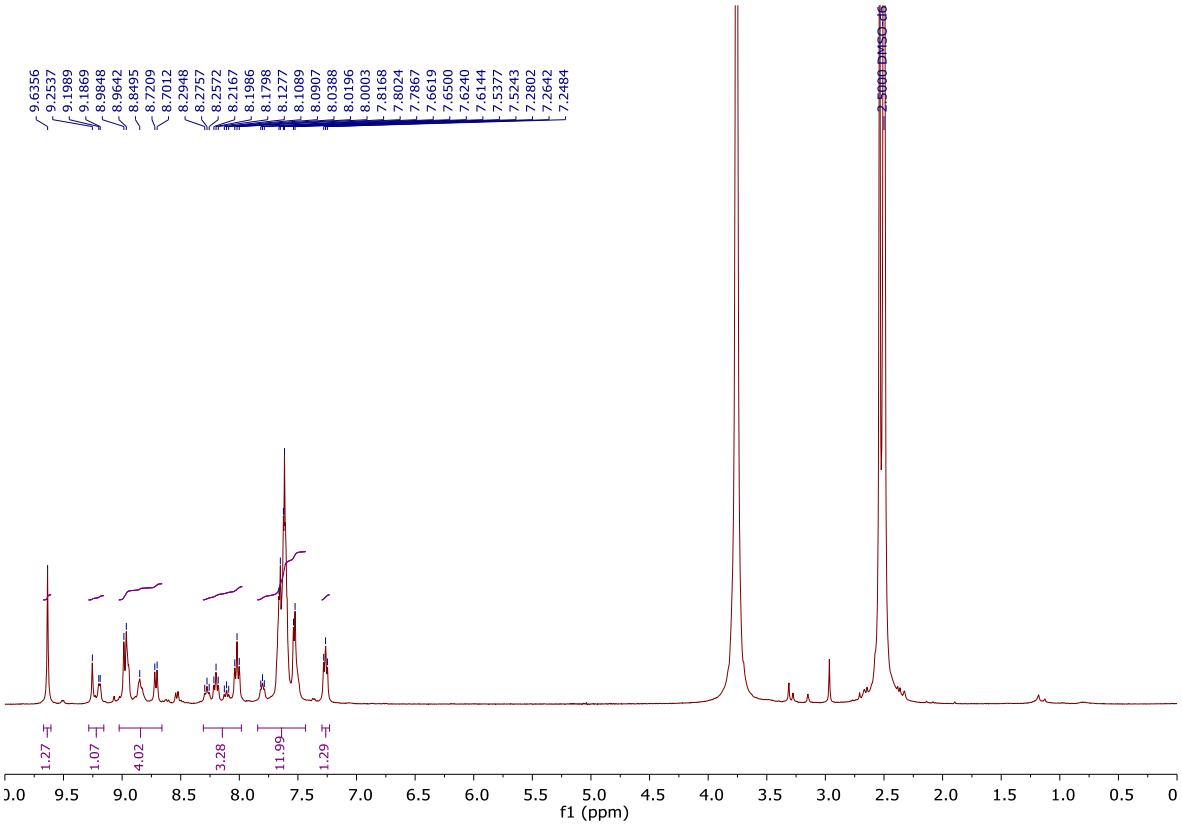

Fig. S11. ^{1}H-NMR spectra of complex **5** (400 MHz, DMSO-d_6) at 298 K.

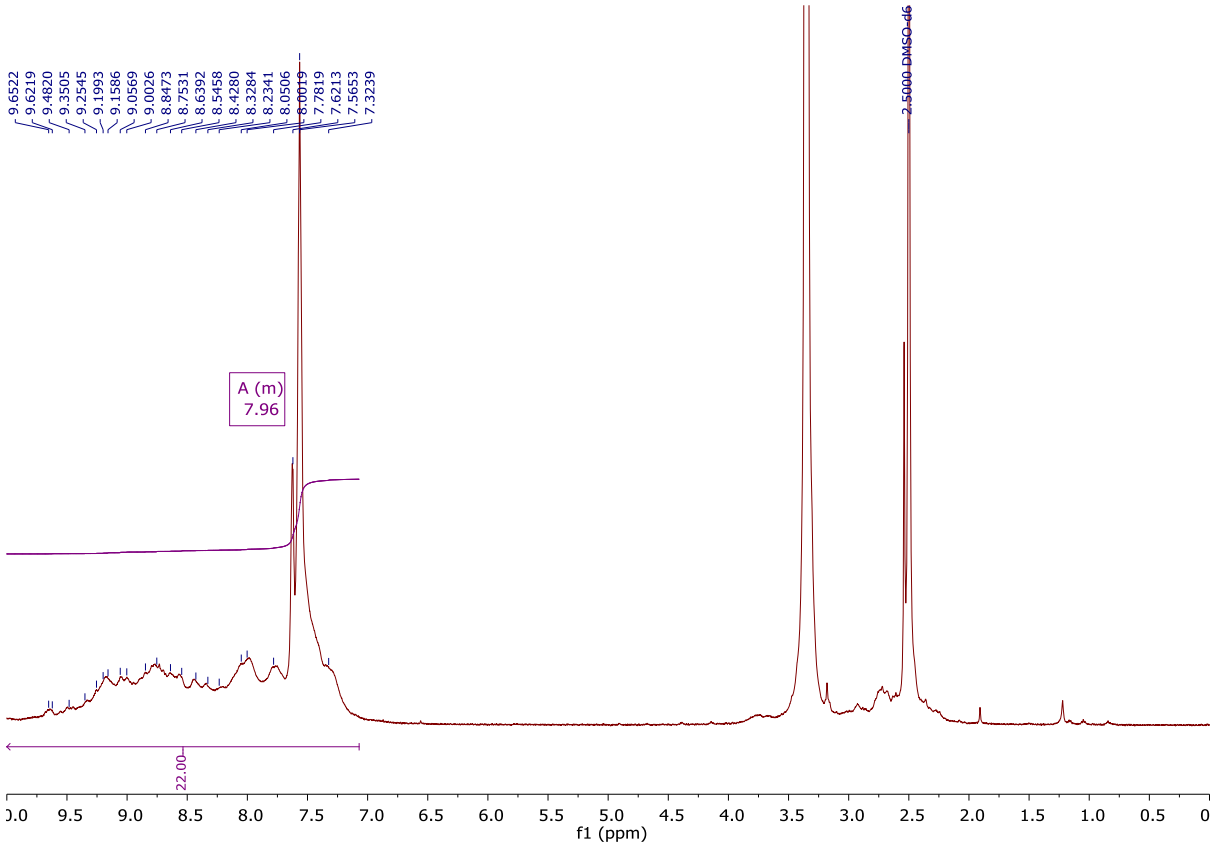

Fig. S12. ^{1}H-NMR spectra of complex **6** (500 MHz, DMSO-d_6) at 298 K.

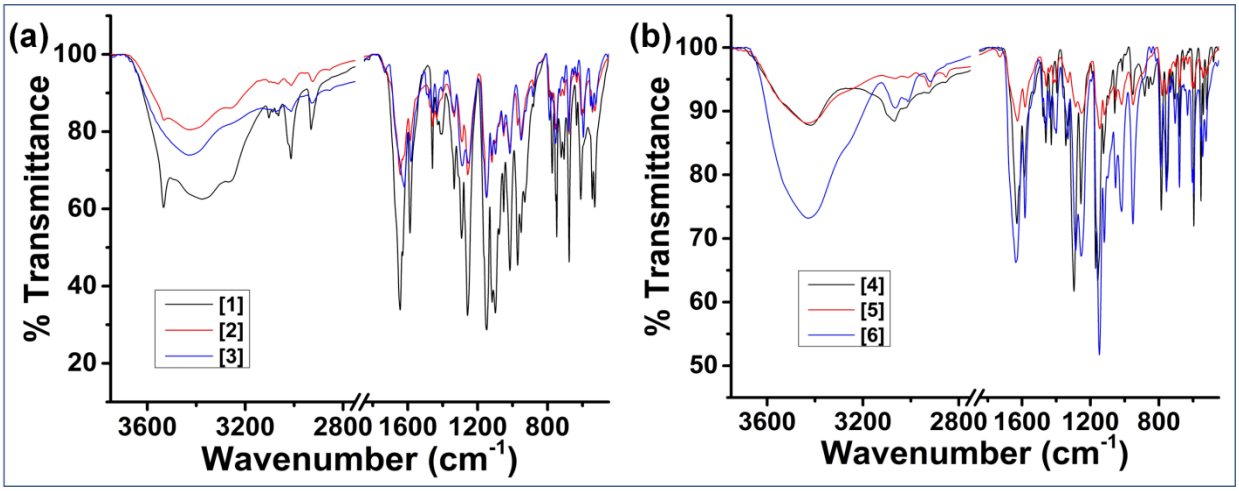

Fig. S13. The solid-state FTIR of complexes in the KBr matrix. (a) Overlay of spectral traces for the complexes **1**–**3**. (b) Overlay of spectral traces for the complexes **4**–**6**.

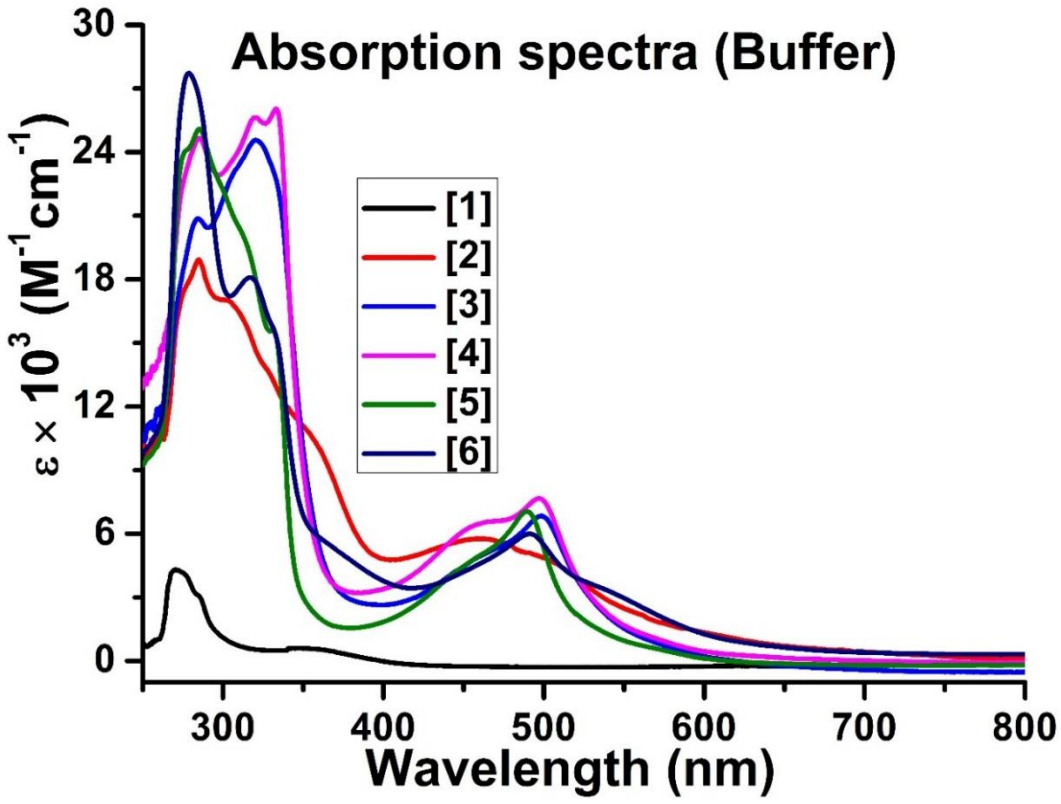

Fig. S14. The absorption spectra of complexes **1**−**6** (20 μM) in 1% (v/v) DMF−5 mM Tris-HCl/NaCl buffer (pH = 7.2) at 298 K.

Table S1. Absorption spectra in 1% (v/v) DMF−5 mM Tris-HCl/NaCl buffer (pH = 7.2) and emission spectra upon 280 nm excitation.

Complex	$\lambda_{max}{}^{a}$/nm, (ε/ $\times 10^3$ $M^{-1}cm^{-1}$)	$\lambda_{em}{}^{b}$
`1	270 (2.12), 344 (0.26)	359, 445
2	285 (18.92), 302 (17.02), 459 (4.82)	345, 451
3	284 (20.86), 322 (22.59), 500 (6.55)	346, 439
4	285 (22.38), 321 (23.04), 333 (2.384), 497 (6.84)	358, 433
5	285 (26.49), 331 (16.14), 489 (7.10)	345, 448
6	279 (25.29), 317 (16.09), 491 (5.14)	359, 450

[a]UV–visible determined absorption peak maximum and molar extinction coefficient in the buffer. [b] Emission maxima with λ_{exc} = 280 nm.

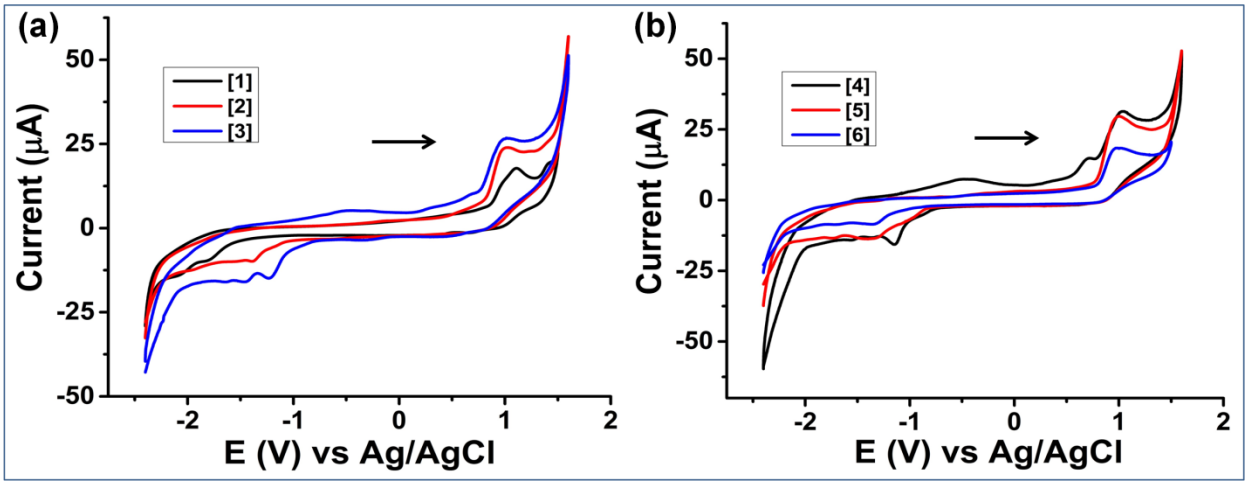

Fig. S15. The cyclic voltammogram for 1 mM DMF solution of complexes (0.1 M $^{n}Bu_4NClO_4$ as supporting electrolyte, glassy carbon working electrode, Pt-wire counter electrode at a scan rate 50 mVs^{-1}. (a) An overlay of spectral traces of the complexes **1**–**3**. (b) An overlay of spectral traces of the complexes **4**–**6**. The arrow shows the scan direction.

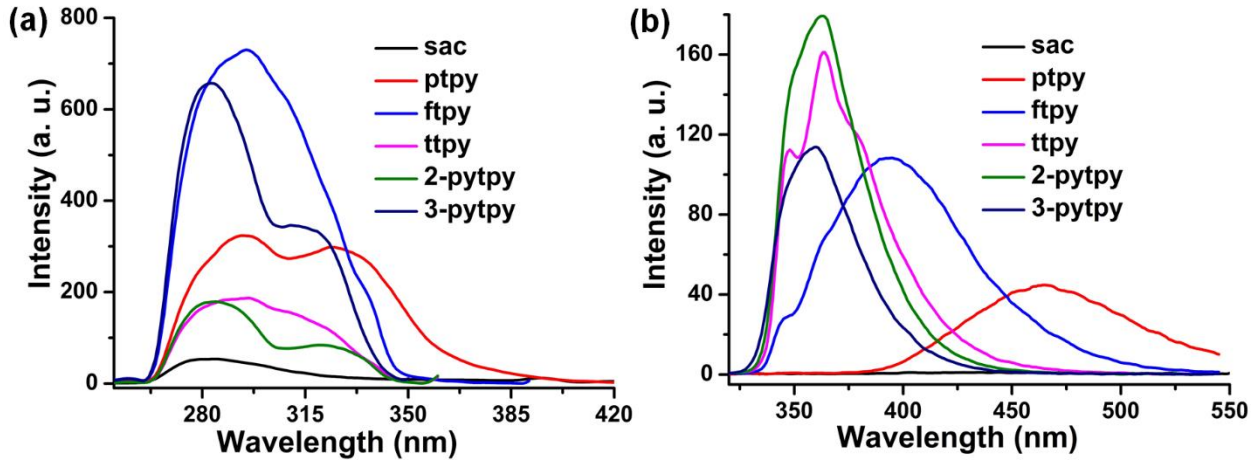

Fig. S16. (a) An overlay of excitation spectra of the ligands (10 μM) in DMF with sac (λ_{em} = 450 nm, exc/em slit = 10/10 nm), ptpy (λ_{em} = 470 nm, exc/em slit = 5/5 nm), ftpy (λ_{em} = 400 nm, exc/em slit = 5/5 nm), ttpy (λ_{em} = 365 nm, exc/em slit = 5/2.5 nm), 2-pytpy (λ_{em} = 365 nm, exc/em slit = 5/5 nm) and 3-pytpy (λ_{em} = 360 nm, exc/em slit = 5/5 nm). (b) An overlay of fluorescence emission spectra of ligands (10 μM) in DMF with λ_{exc} = 280 nm (exc/em slit = 5/2.5 nm).

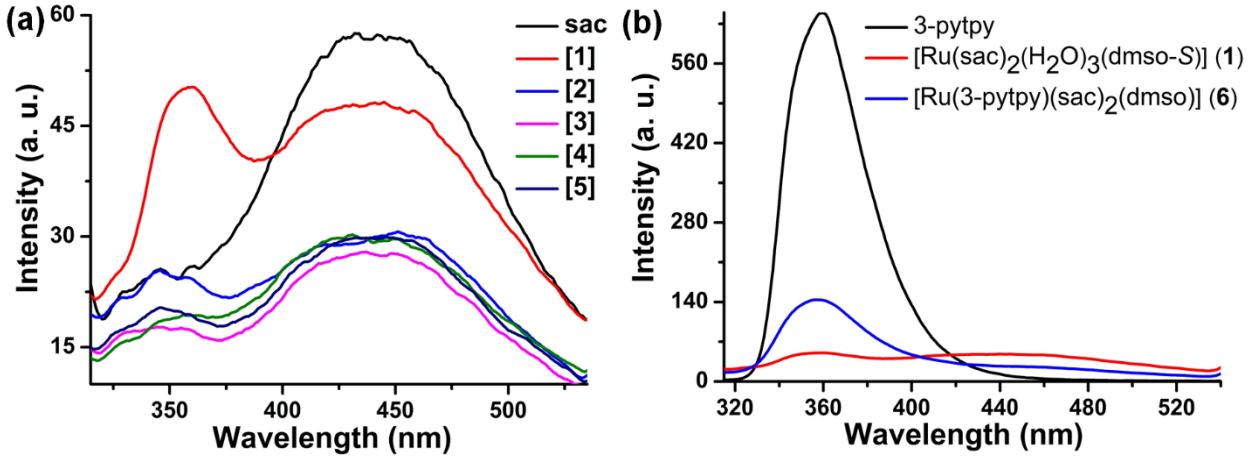

Fig. S17. (a) Overlay of fluorescence spectra (λ_{ex} = 280 nm) of the **sac** and complexes **1–5** (10 μM) each in DMF with exc/em slit = 10/10 nm. (b) Overlay of fluorescence emission spectra (λ_{ex} = 280 nm) of the **3-pytpy** and complexes **1** and **6** (10 μM) each in DMF with exc/em slit = 10/10 nm for complexes and 5/5 nm for **3-pytpy**.

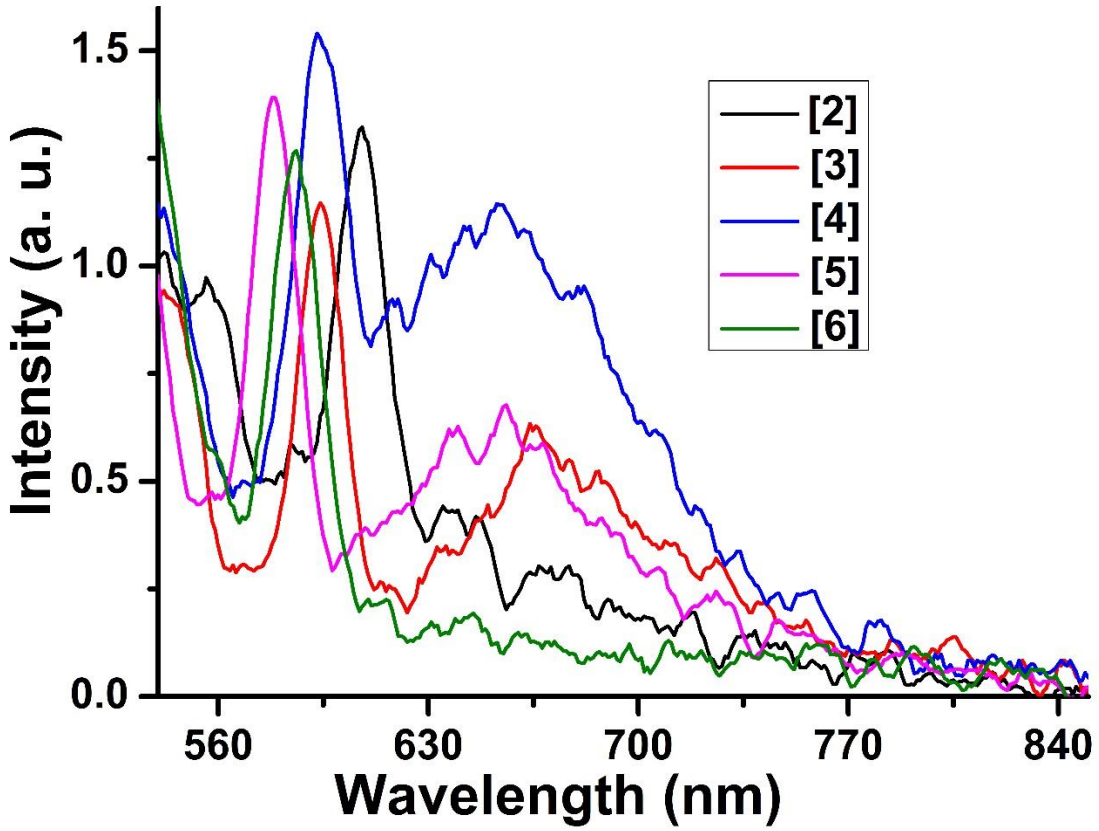

Fig. S18. The emission spectra of the complexes **2**-**6** (10 μM) in DMF upon photoexcitation of MLCT bands: 515 nm (**2**), 505 nm (**3**), 505 nm (**4**), 495 nm (**5**) and 500 nm (**6**). [ex. slit width = 10 nm, em. slit width = 10 nm, T = 298 K]

Table S2. Selected crystallographic data and structure refinement parameters for complexes **1**, **3**, **4**, and **5**.

Parameters	**1**	**3**	**4**	**5**
Empirical formula	$C_{16}H_{20}N_2O_{10}RuS_3$	$C_{35}H_{24}N_6O_7RuS_2$	$C_{33}H_{23}N_5O_7RuS_3$	$C_{34}H_{24}N_6O_7RuS_2$
M_r	597.59	808.79	798.81	793.78
crystal system	Triclinic	Triclinic	Triclinic	Triclinic
space group	*P*-1	*P*-1	*P*-1	*P*-1
a(Å)	7.0672(7)	12.0014(6)	11.5927(18)	11.0081(7)
b(Å)	7.7987(7)	12.1514(6)	13.445(2)	13.9727(9)
c (Å)	20.999(2)	12.9911(7)	13.715(2)	14.7973(10)
α (deg)	88.464(2)	76.775(2)	78.814(3)	70.839(2)
β(deg)	84.971(2)	86.439(2)	67.894(3)	75.280(2)
γ(deg)	71.780(2)	74.9130(10)	68.326(3)	82.782(2)
Volume (Å^3)	1095.09(18)	1780.72(16)	1836.8(5)	2077.1(2)
Z	2	2	2	2
ρ_{calc}g/cm^3	1.812	1.503	1.444	1.269
μ (mm^{-1})	1.059	0.614	0.648	0.525
F(000)	604.0	816.0	808.0	804.0
T(K)	273.15	273.15	273.15	273.15
2θ range for data collection(deg)	5.5 to 56.752	5.302 to 50.1	4.31 to 49.0	5.37 to 56.834
Limiting indices	$-9 \le h \le 9$, $-10 \le k \le 10$, $-28 \le l \le 28$	$-14 \le h \le 14$, $-14 \le k \le 14$, $-15 \le l \le 15$	$-13 \le h \le 13$, $-16 \le k \le 16$, $-16 \le l \le 16$	$-14 \le h \le 14$, $-18 \le k \le 18$, $-19 \le l \le 19$
Reflections collected	15890	21765	13300	31208
unique reflections	5477	6316	6041	10375
R(int)	0.0632	0.0636	0.1219	0.0793
T_{max}/T_{min}	0.746/0.642	0.746/0.648	0.746/0.652	0.746/0.649
Data/restraints/parameters	477/0/294	6316/0/461	6041/5/395	10375/0/452
GOF on F^2	1.131	1.018	0.980	0.981
R_1[a] and wR_2[b] [$I>2\sigma(I)$]	$R1$ = 0.0592, $wR2$ = 0.1200	$R1$ = 0.0456, $wR2$ = 0.1069	$R1$ = 0.0897, $wR2$ = 0.1762	$R1$ = 0.0623, $wR2$ = 0.1343
R_1 and wR_2 (all data)	$R1$ = 0.0858, $wR2$ = 0.1283	$R1$ = 0.0657, $wR2$ = 0.1143	$R1$ = 0.1701, $wR2$ = 0.2069	$R1$ = 0.1059, $wR2$ = 0.1492
Largest diff. peak/hole (eÅ^{-3})	1.08/-1.05	1.10/-0.55	1.49/-0.99	1.29/-0.72
CCDC deposition serial number	2057838	2057839	2057840	2057841

[a]$R_1 = \Sigma||F_o|-|F_c||/\Sigma|F_o|$; [b]$wR_2 = \{\Sigma[w(F_o^2-F_c^2)^2]/\Sigma[w(F_o^2)^2]\}^{1/2}$. Goodness-of-fit (GOF) = $\{\Sigma[w(F_o^2-F_c^2)^2/(n-p)]\}^{1/2}$, where n = number of data and p = number of parameters refined.

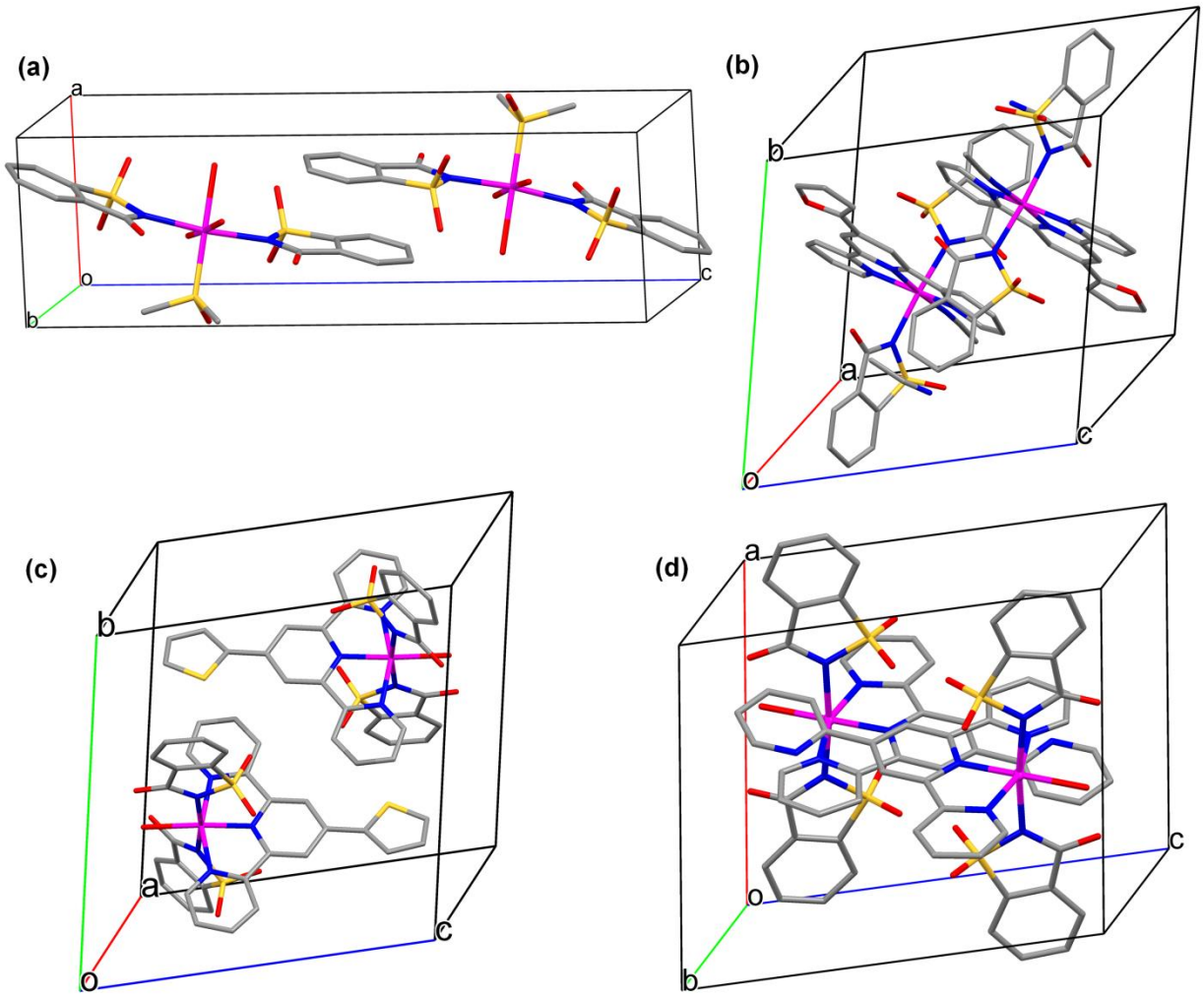

Fig. S19. Unit cell diagrams for the complexes (a) **1**, (b) **3**, (c) **4** and (d) **5**

Table S3. Selected bond lengths and bond angles for complexes **1** and **3** from their crystal structures

Bond lengths (Å) (**1**)		Bond lengths (Å) (**3**)	
Ru1-S3	2.1831(12)	Ru-N4	1.944(3)
Ru1-O3	2.117(4)	Ru1-N5	2.064(3)
Ru1-N1	2.141(4)	Ru1-N6	2.038(3)
Ru1-N2	2.128(4)	Ru1-N2	2.124(3)
Ru1-O2	2.168(4)	Ru1-N1	2.134(3)
Ru1-O1	2.143(4)	Ru1-N3	2.078(3)
Bond Angles (deg)		**Bond Angles (deg)**	
O3-Ru1-S3	96.53(10)	N4-Ru1-N5	79.67(13)
O3-Ru1-N1	87.54(15)	N4-Ru1-N6	175.67(13)
O3-Ru1-N2	88.03(15)	N4-Ru1-N2	88.90(12)
O3-Ru1-O2	85.96(16)	N4-Ru1-N1	94.20(14)
O3-Ru1-O1	176.39(15)	N4-Ru1-N3	78.70(13)
N1-Ru1-S3	90.93(11)	N5-Ru1-N2	90.04(12)
N1-Ru1-O2	88.41(15)	N5-Ru1-N1	88.20(13)
N1-Ru1-O1	92.10(16)	N5-Ru1-N3	157.95(13)
N2-Ru1-S3	94.60(12)	N6-Ru1-N5	102.17(13)
N2-Ru1-N1	173.27(16)	N6-Ru1-N2	87.19(13)
N2-Ru1-O2	86.23(16)	N6-Ru1-N1	89.79(13)
N2-Ru1-O1	92.00(16)	N6-Ru1-N3	99.70(13)
O2-Ru1-S3	177.40(13)	N2-Ru1-N1	176.11(13)
O1-Ru1-S3	87.07(12)	N3-Ru1-N2	93.78(13)
O1-Ru1-O2	90.44(17)	N3-Ru1-N1	89.14(13)

Table S4. Selected bond lengths and bond angles for the complexes **4** and **5** from the X-ray structures

Bond lengths (Å) (**4**)		Bond lengths (Å) (**5**)	
Ru1-O7	2.191(6)	Ru1-O7	2.174(2)
Ru1-N5	2.081(7)	Ru1-N5	2.063(3)
Ru1-N4	1.927(7)	Ru1-N4	1.921(3)
Ru1-N2	2.147(8)	Ru1-N1	2.121(3)
Ru1-N3	2.075(8)	Ru1-N3	2.059(3)
Ru1-N1	2.131(8)	Ru1-N2	2.114(3)
Bond Angles (deg)		**Bond Angles (deg)**	
N5-Ru1-O7	101.5(3)	N5-Ru1-O7	101.65(11)
N5-Ru1-N2	88.2(3)	N5-Ru1-N1	89.54(12)
N5-Ru1-N1	89.9(3)	N5-Ru1-N2	89.28(12)
N4-Ru1-O7	176.5(3)	N4-Ru1-O7	177.56(12)
N4-Ru1-N5	80.4(3)	N4-Ru1-N5	80.43(13)
N4-Ru1-N2	91.9(3)	N4-Ru1-N1	92.91(12)
N4-Ru1-N3	79.8(3)	N4-Ru1-N3	80.06(13)
N4-Ru1-N1	95.3(3)	N4-Ru1-N2	93.40(12)
N2-Ru1-O7	85.2(3)	N1-Ru1-O7	88.40(11)
N3-Ru1-O7	98.4(3)	N3-Ru1-O7	97.85(11)
N3-Ru1-N5	160.1(3)	N3-Ru1-N5	160.49(12)
N3-Ru1-N2	172.2(3)	N3-Ru1-N1	91.10(12)
N3-Ru1-N1	89.7(3)	N3-Ru1-N2	92.20(12)
N1-Ru1-O7	87.7(3)	N2-Ru1-O7	85.38(11)
N1-Ru1-N2	172.2(3)	N2-Ru1-N1	173.30(12)

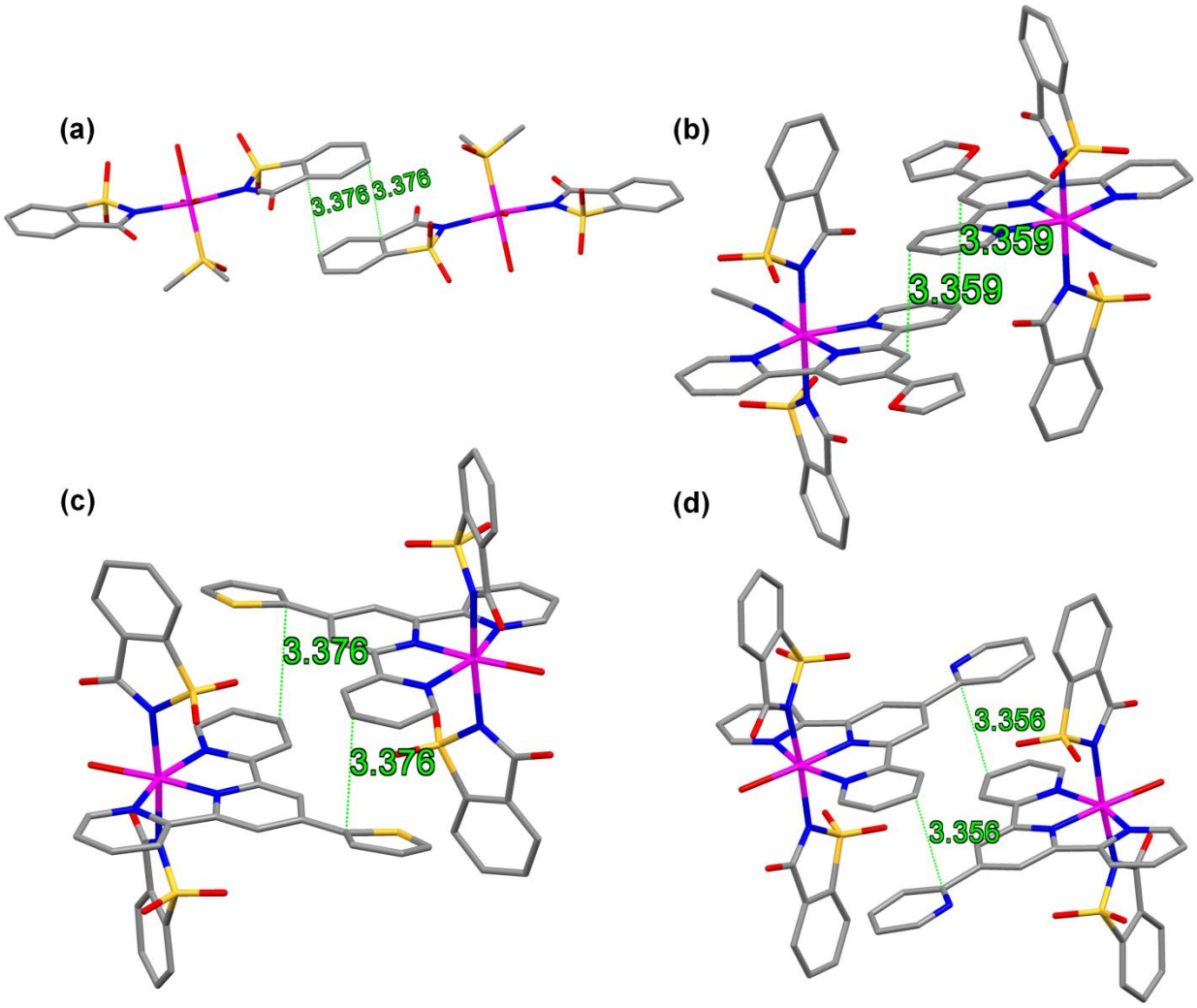

Fig. S20. The strong π–π interactions in aromatic rings of the complexes **1** (a), **3** (b), **4** (c), and **5** (d) at a distance marked (Å) from X-ray structure studies.

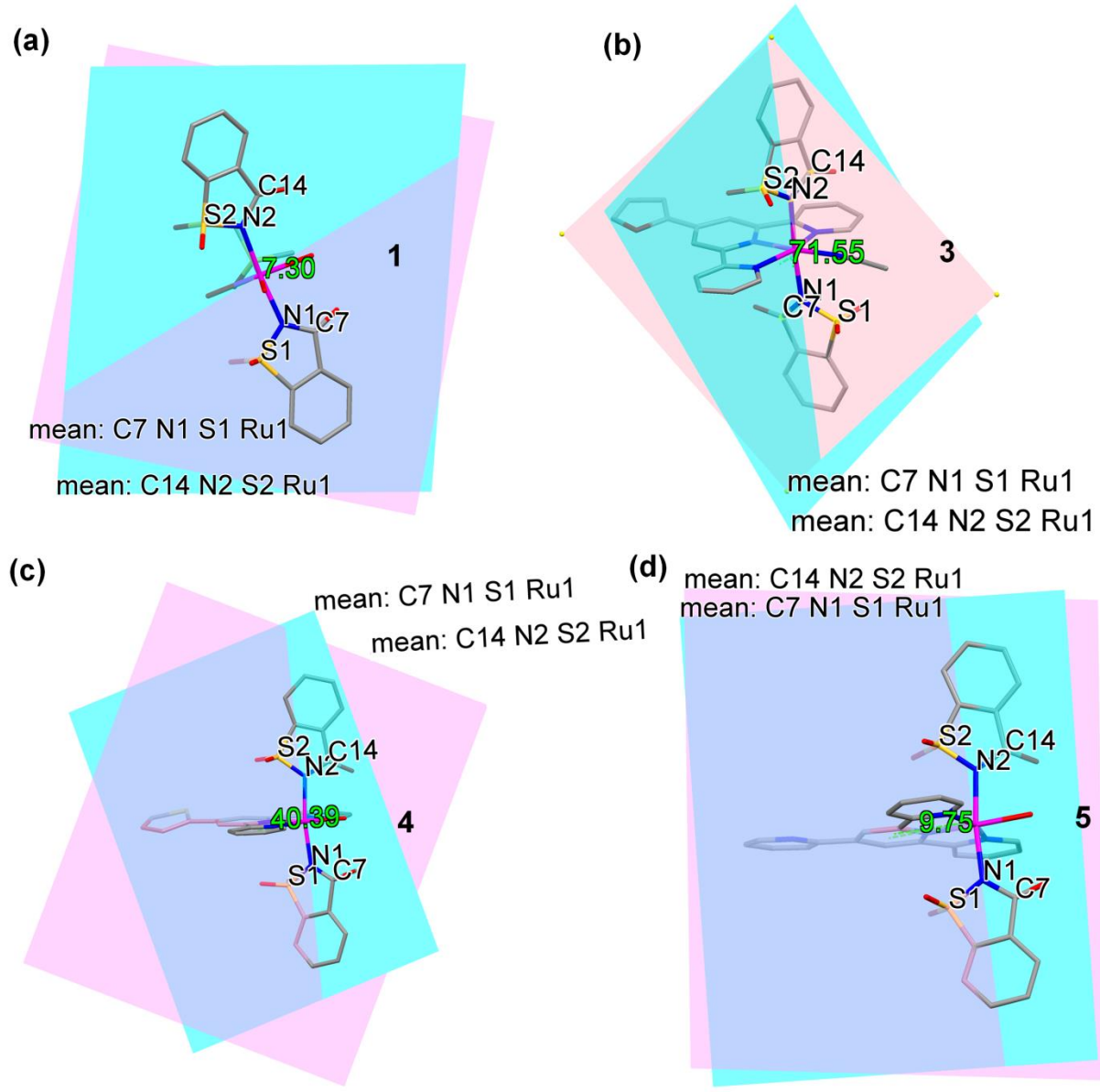

Fig. S21. The angle between the planes containing saccharinates ligands in complexes (a) **1**, (b) **3**, (c) **4**, and (d) **5**

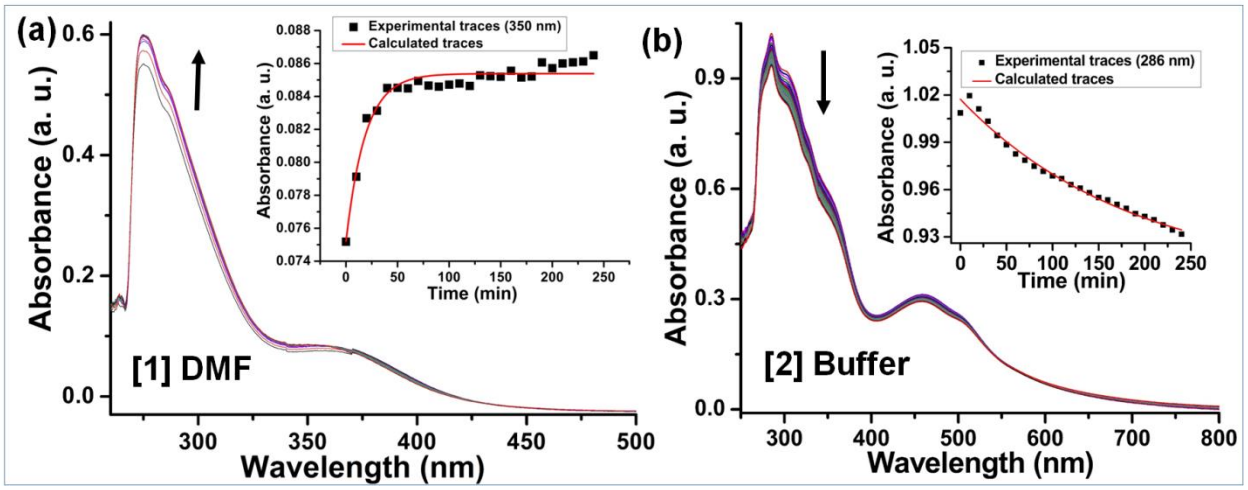

Fig. S22. The electronic absorption changes of the complexes upon solvation for 240 mins in dark**.** (a) Complex **1** (198 μM) in DMF. Inset: The first-order kinetic fit of the changes in the absorbance of complex **1** at 350 nm. (b) The hydrolysis of complex **2** (58 μM) in 3% (v/v) DMF-5 mM Tris-HCl/NaCl buffer (pH = 7.2) mixture. Inset: The first-order kinetic fit of the changes in the absorbance of complex **2** at 286 nm upon hydrolysis.

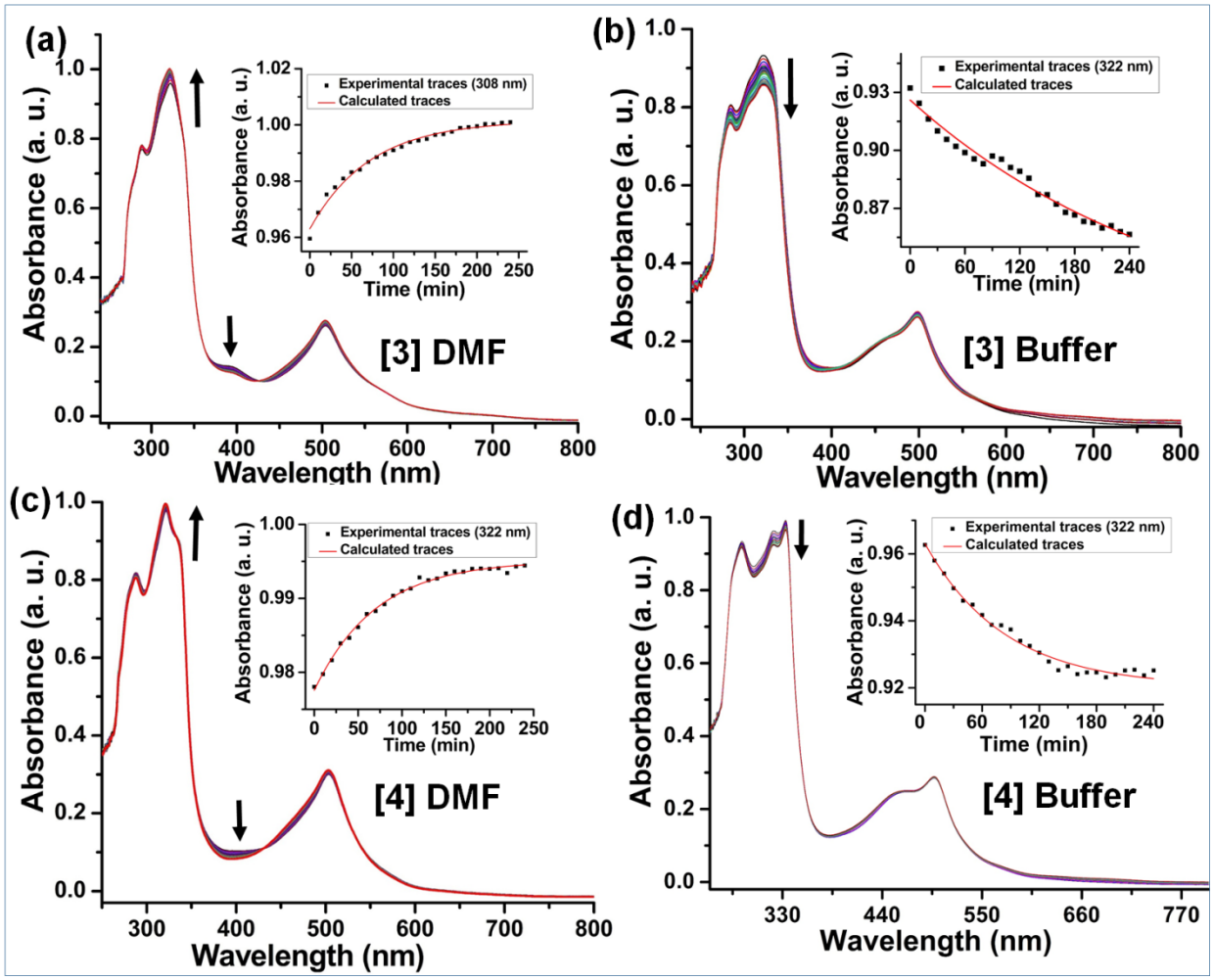

Fig. S23. The electronic absorption changes of the complexes (39 μM) **3** and **4** upon solvation for 240 mins in DMF and 2% (v/v) DMF-5 mM Tris-HCl/NaCl buffer (pH = 7.2) mixture in dark. (a) Complex **3**. (b) The hydrolysis of complex **3**. (c) Complex **4**. (d) The hydrolysis of complex **4**. Inset (a)−(d) The first-order kinetic fit of the changes in the absorbance of complexes upon solvation.

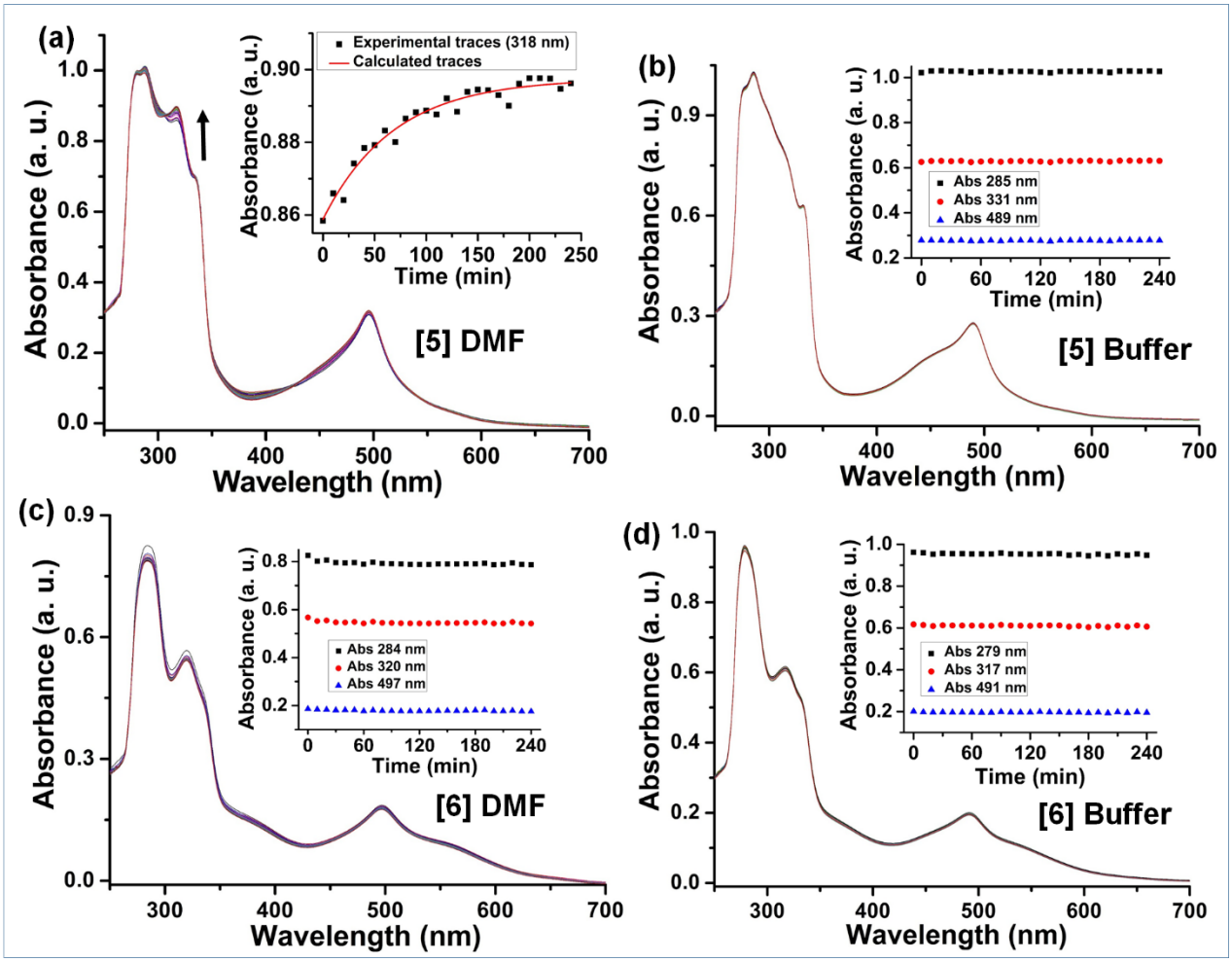

Fig. S24. The electronic absorption changes of the complexes **5** and **6** upon solvation for 240 mins in DMF and 2% (v/v) DMF-5mM Tris-HCl/NaCl buffer (pH = 7.2) mixture in dark**.** (a) Complex **5** (39 μM). Inset: The first-order kinetic fit of the changes in the absorbance of complex **5** at 318 nm. (b) The hydrolysis of complex **5** (39 μM). (c) Complex **6** (30 μM). (d) The hydrolysis of complex **6** (39 μM). Insets (b)−(d) show changes in specified wavelengths with time.

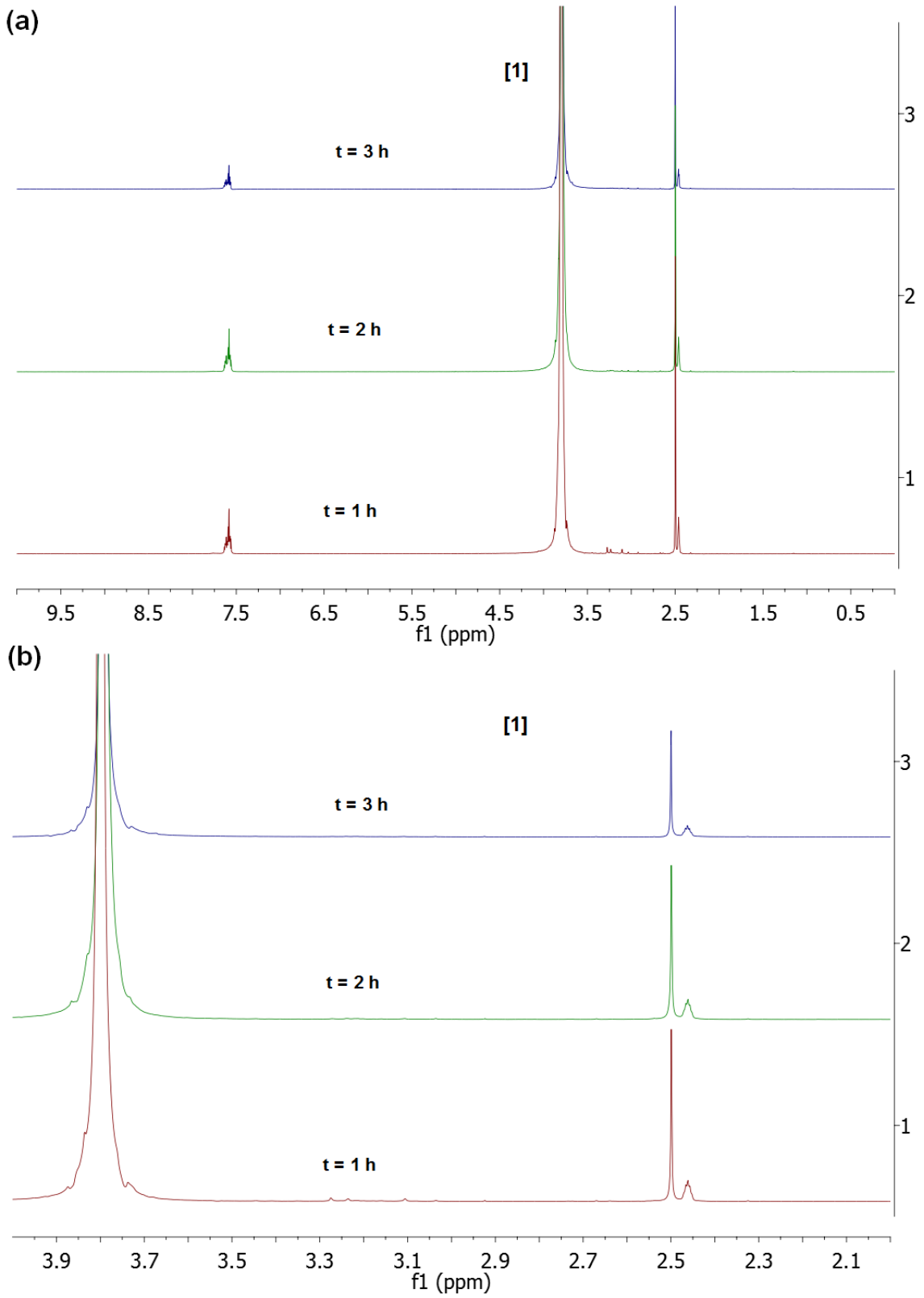

Fig. S25. Time-dependent ^{1}H-NMR spectra of the complex **1** (DMSO-d_6, 400 MHz). (a) Overlay region 0–10 ppm, (b) Overlay region 2.0–4.0 ppm.

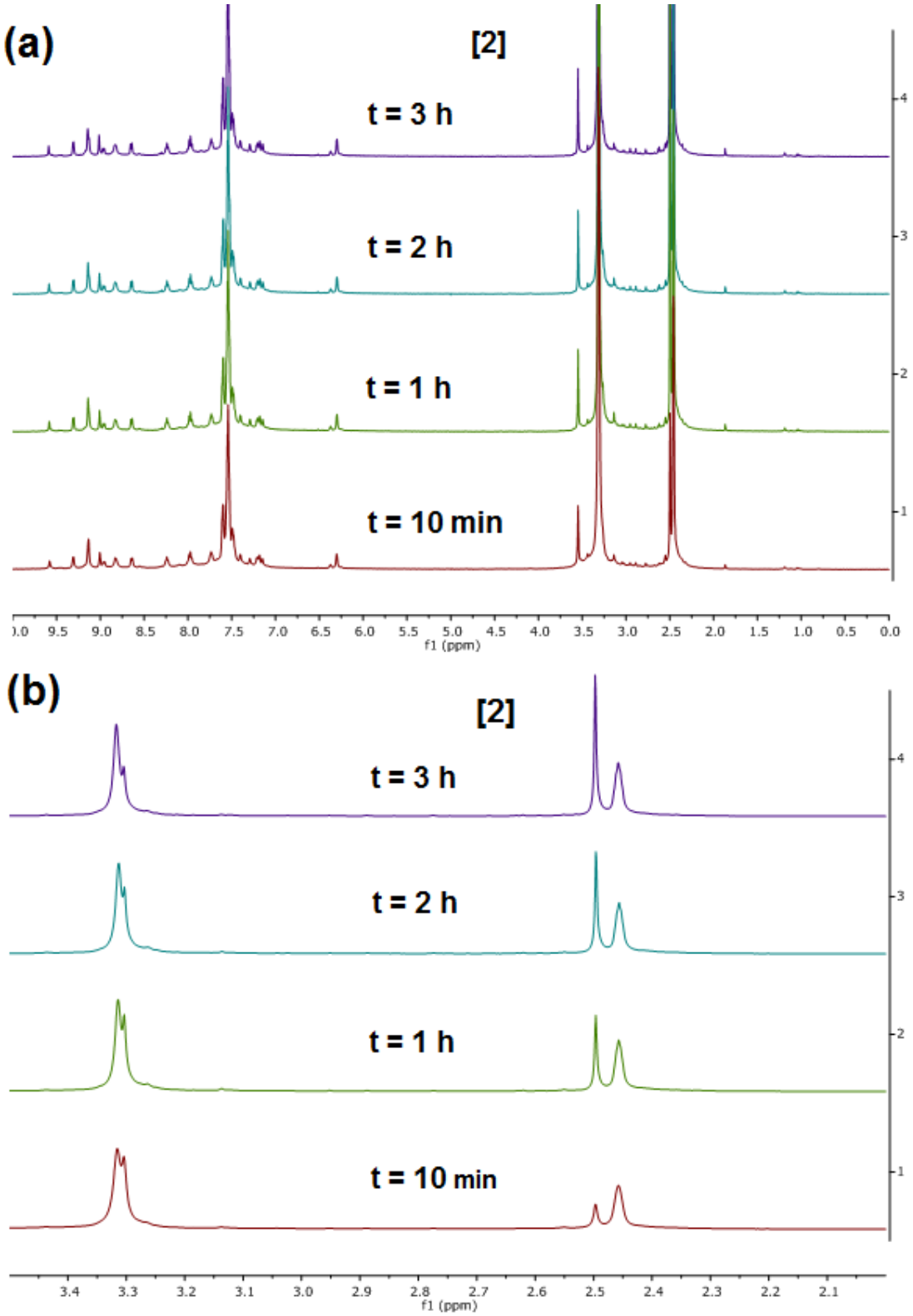

Fig. S26. Time-dependent concomitant evolution of ^{1}H-NMR spectra of the complex **2** (DMSO-d_6, 500 MHz). (a) Overlay region: 0–10 ppm, (b) Overlay region: 2.0–3.5 ppm.

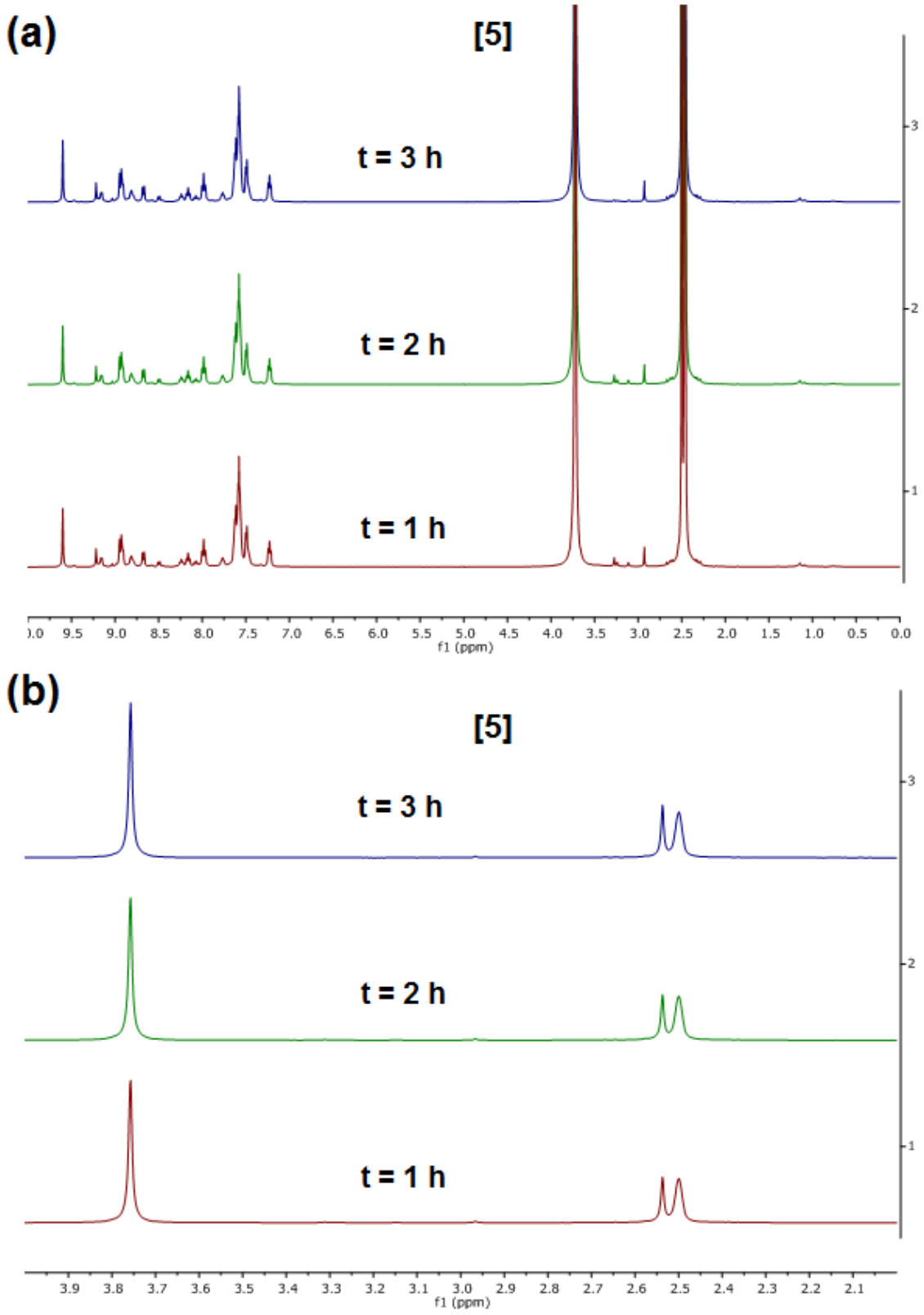

Fig. S27. Time-dependent concomitant evolution of ^{1}H-NMR spectra of the complex **5** (DMSO-d_6, 500 MHz). (a) Overlay region: 0–10 ppm, (b) Overlay region: 2.0–3.5 ppm.

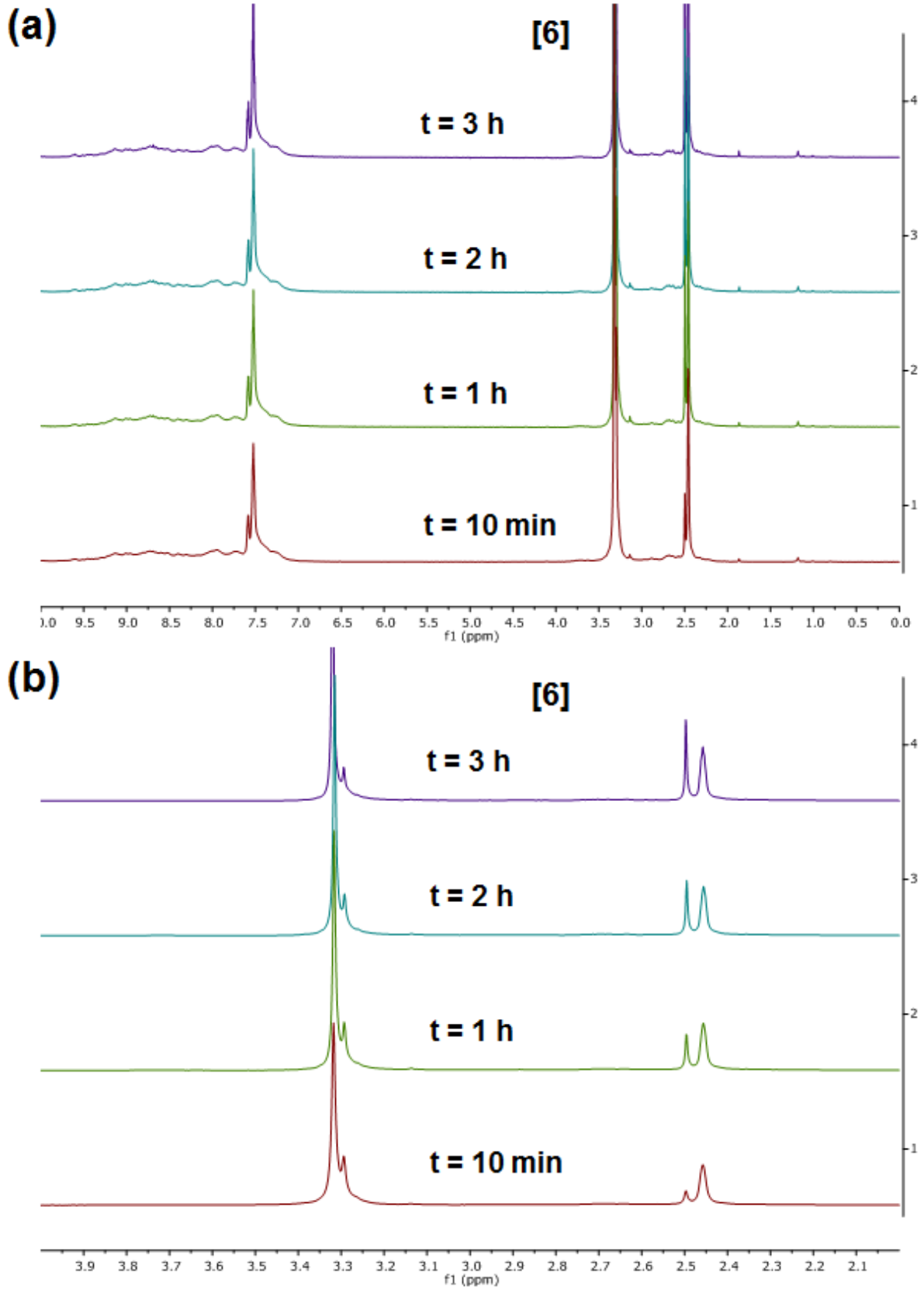

Fig. S28. Time-dependent concomitant evolution of ^{1}H-NMR spectra of the complex **5** (DMSO-d_6, 500 MHz). (a) Overlay region: 0–10 ppm, (b) Overlay region: 2.0–3.5 ppm.

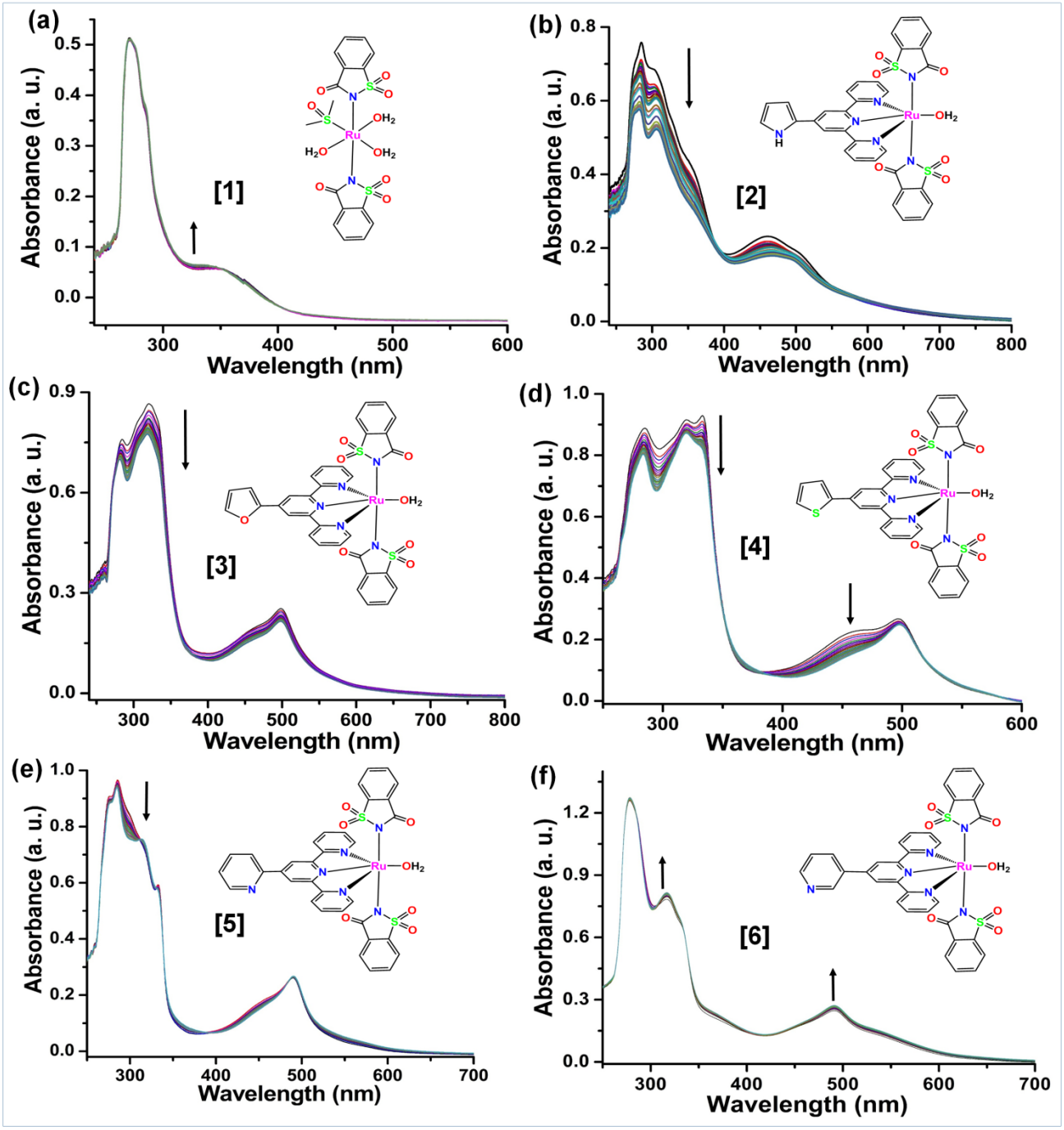

Fig. S29. The effect of white light (WL) irradiation (λ_{ex} > 400 nm, 5V, 0.3 W) upon complexes. (a) **1** (214 μM); (b)−(f) **2**−**6** (39 μM) in the DMF-5mM Tris-HCl/NaCl buffer (pH = 7.2) mixture (12% (v/v) for **1** and 2% (v/v) for **2**−**6**) for 0−100 min. The direction of changes in UV-visible spectral traces was indicated with arrow.

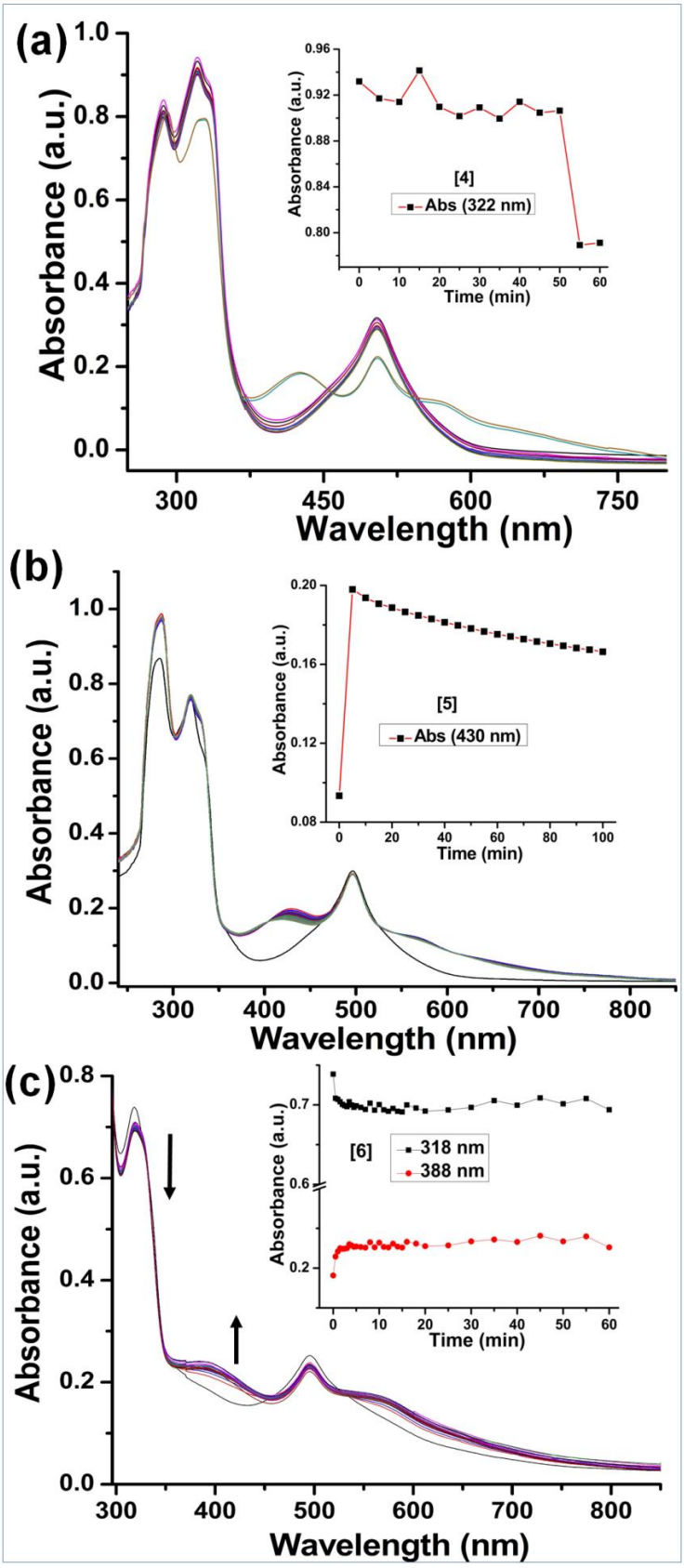

Fig. S30. The green light (λ_{ex} = 530 nm) LED (3V, 158 lm @ 700mA) induced changes in the electronic spectral traces of the complexes and inset shows the changes in absorbance of selected wavelength vs time. (a) Complex **4** (39 μM) for 0−60 min. (b) Complex **5** (39 μM) for 0−100 min. (a) Complex **6** (39 μM) for 0−60 min.

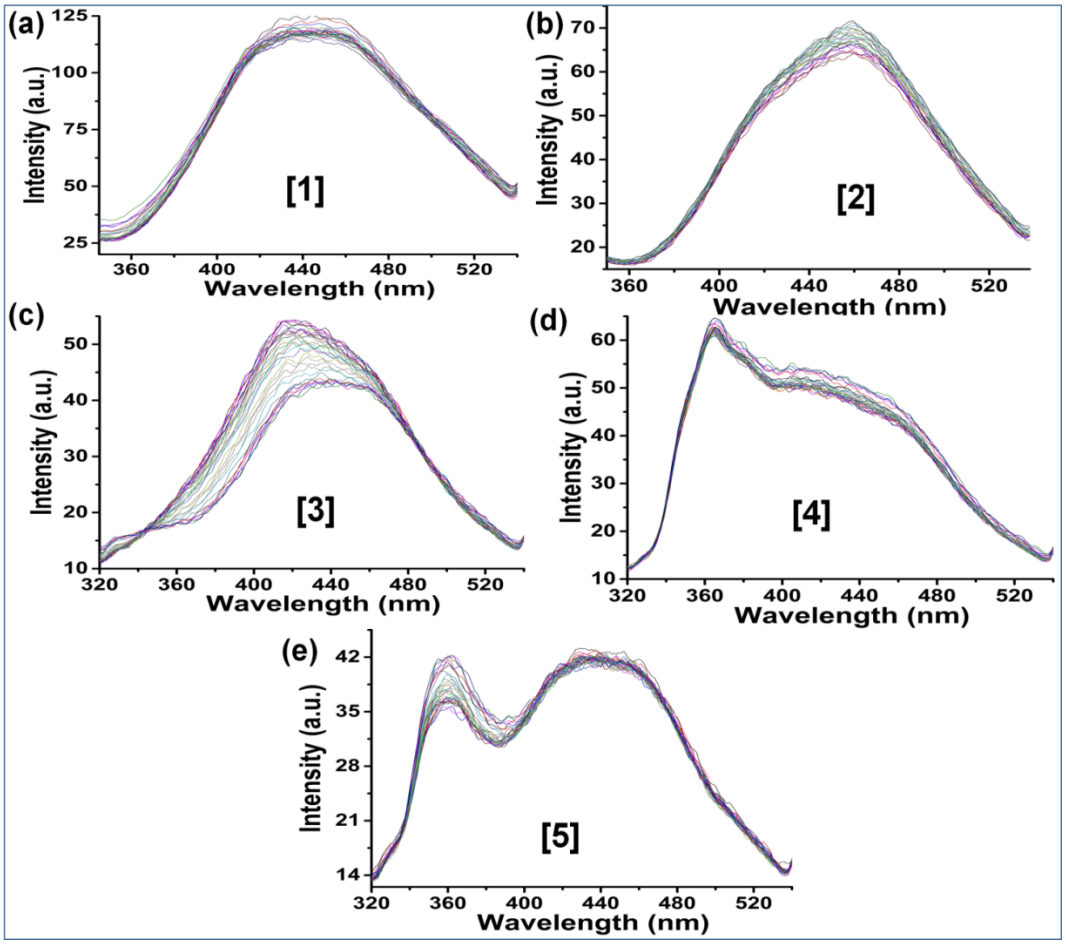

Fig. S31. The monitoring of fluorescence spectra of the complexes **1**−**5** (20 μM) upon green light (λ_{ex} = 530 nm) LED (3V, 158 lm @ 700 mA) irradiation for 0−60 min. Ex. slit width = 10 nm, em. slit width = 10 nm, T = 298 K.

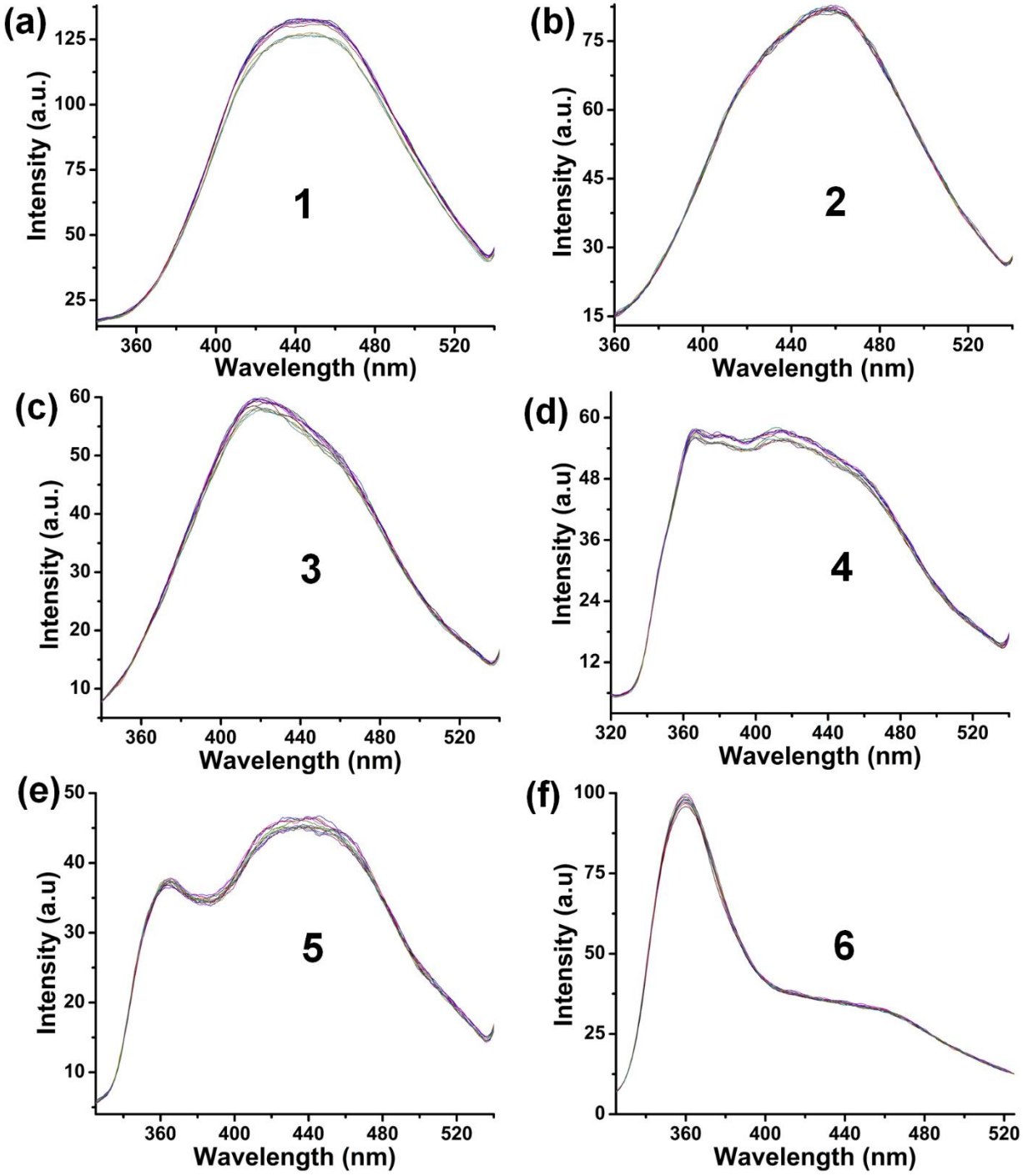

Fig. S32. Fluorescence spectra (λ_{ex} = 280 nm) of the complexes **1**–**6** (20 μM) in the dark for 0−60 min. Ex. slit width = 10 nm, em. slit width = 10 nm, T = 298 K.

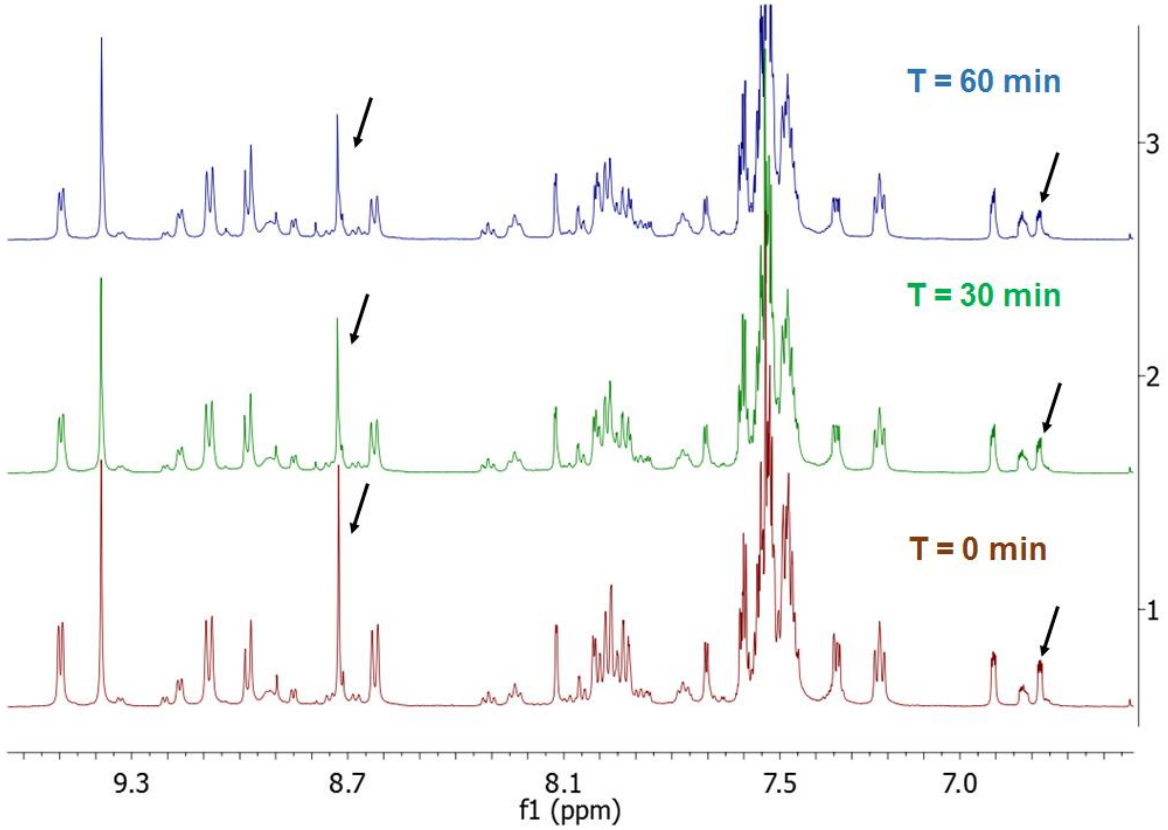

Fig. S33. Greenlight (λ_{ex} = 530 nm) induced ^{1}H-NMR spectra of the complex **3** (DMSO-d_6, 500 MHz) for 30 min (green traces) and 60 min (blue trace).

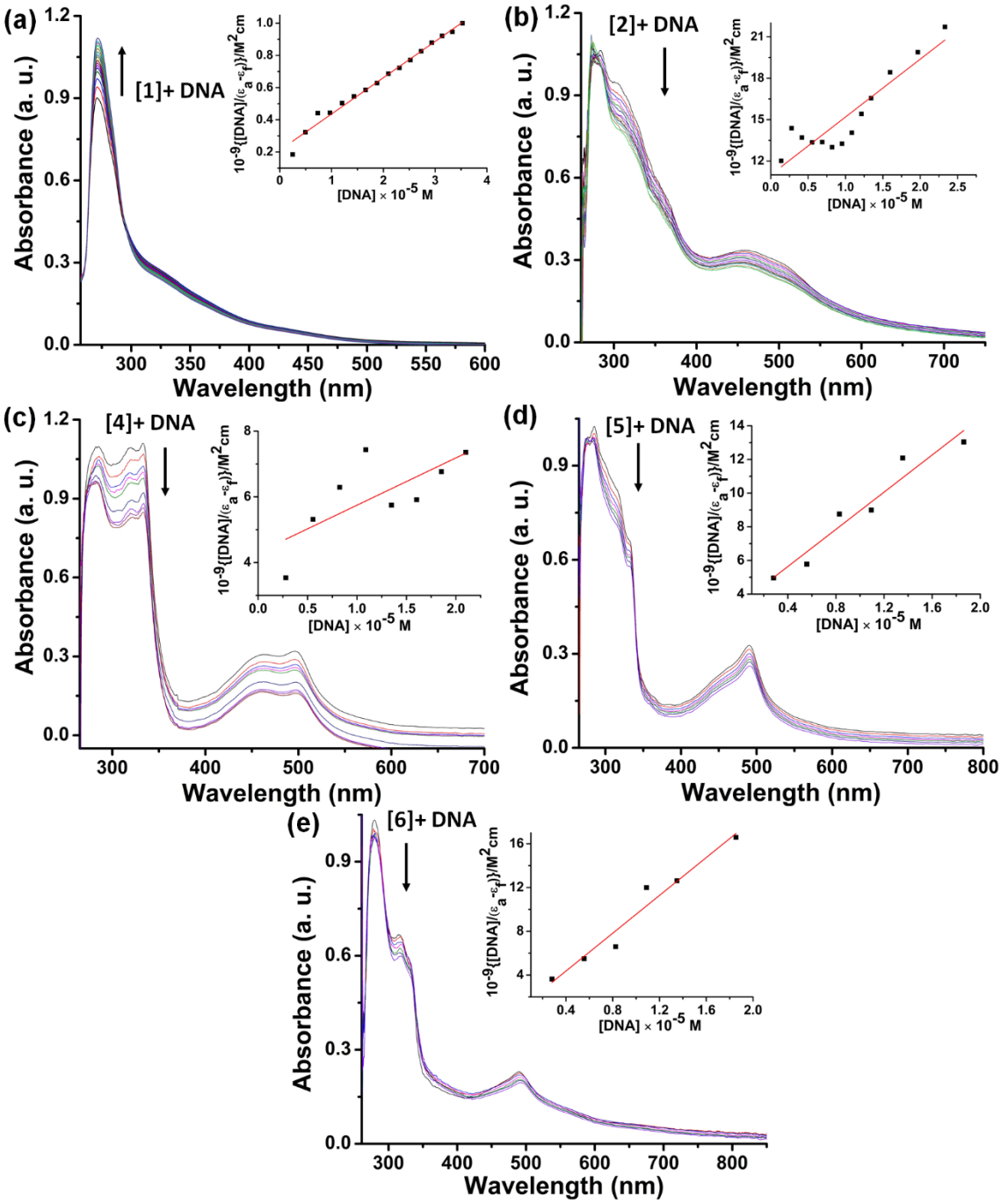

Fig. S34. The binding interaction of the complexes with CT-DNA in 5mM Tris-HCl/NaCl buffer (pH = 7.2) lead to hyperchromism (**1**) and hypochromism for **2**−**6** of their absorption bands. (a) **1** (268 μM) with DNA (0−35 μM) in 12% (v/v) DMF-buffer mixture. (b) **2** (58 μM) with DNA (0−23 μM) in 2.7% (v/v) DMF−buffer mixture. (c) **4** (49 μM) with DNA (0−21 μM) in 2.3% (v/v) DMF-buffer mixture (d) **5** (39 μM) with DNA (0−19 μM) in 1.8% (v/v) DMF−buffer (e) **6** (49 μM) with DNA (0−19 μM) in 2.3% (v/v) DMF−buffer. Inset (a)−(e) Plot [DNA]/$\Delta\varepsilon_{af}$ *vs.* [DNA] for the corresponding complexes in each plot.

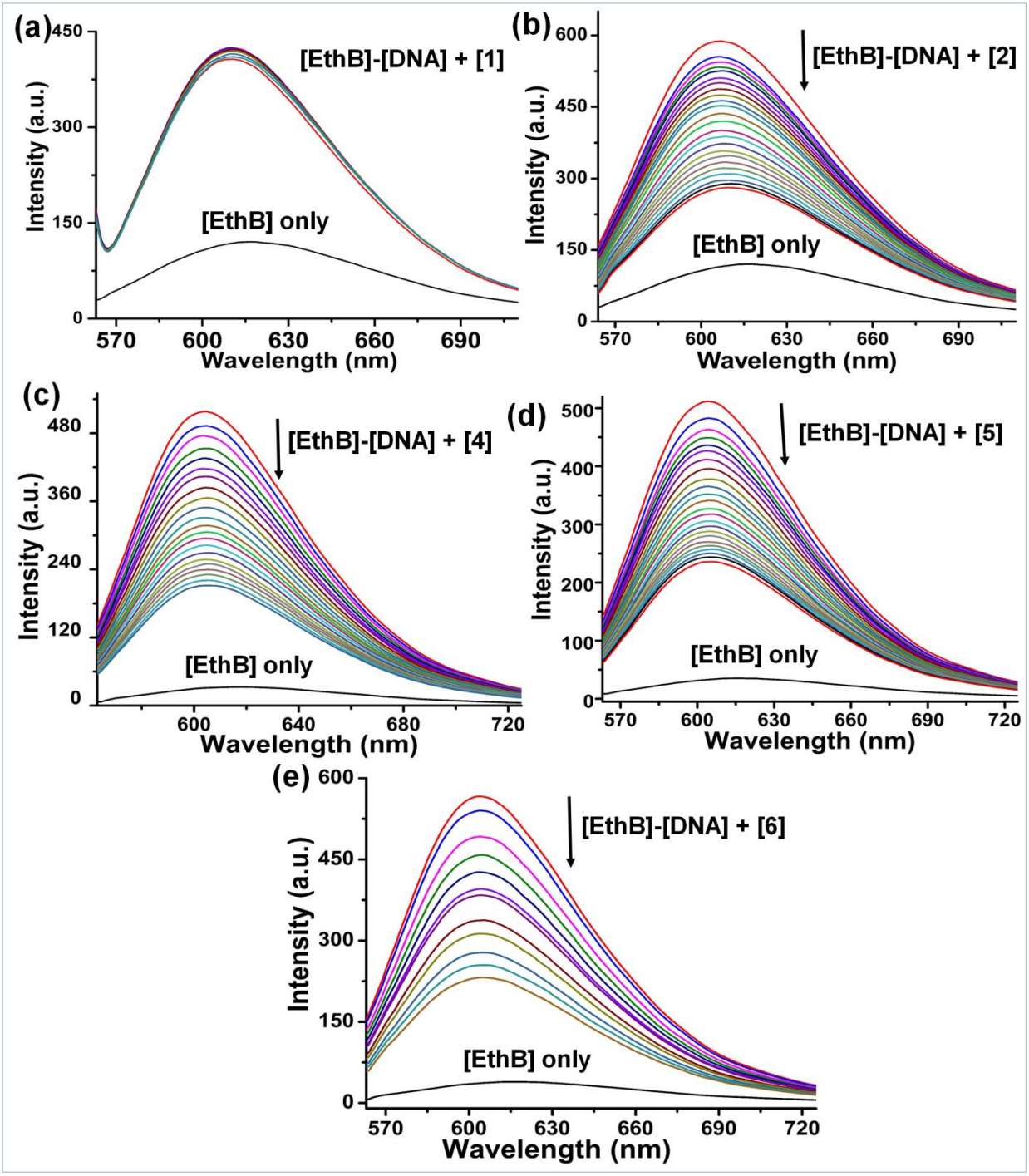

Fig. S35. Ethidium bromide (EthB) displacement assay for the complexes. The gradual addition of (a) complex **1** (0−66 μM); (b) complex **2** (0−66 μM); (c) complex **4** (0−39 μM); (d) complex **5** (0−42 μM) and (e) complex **6** (0−20 μM) to the multi-step pretreated EthB (12 μM) with CT-DNA (14.4 μM) addition lead to significant quenching of fluorescence intensity of the adduct ~ 605 nm. Ex. slit width = 10 nm, em. slit width = 10 nm, T = 298 K.

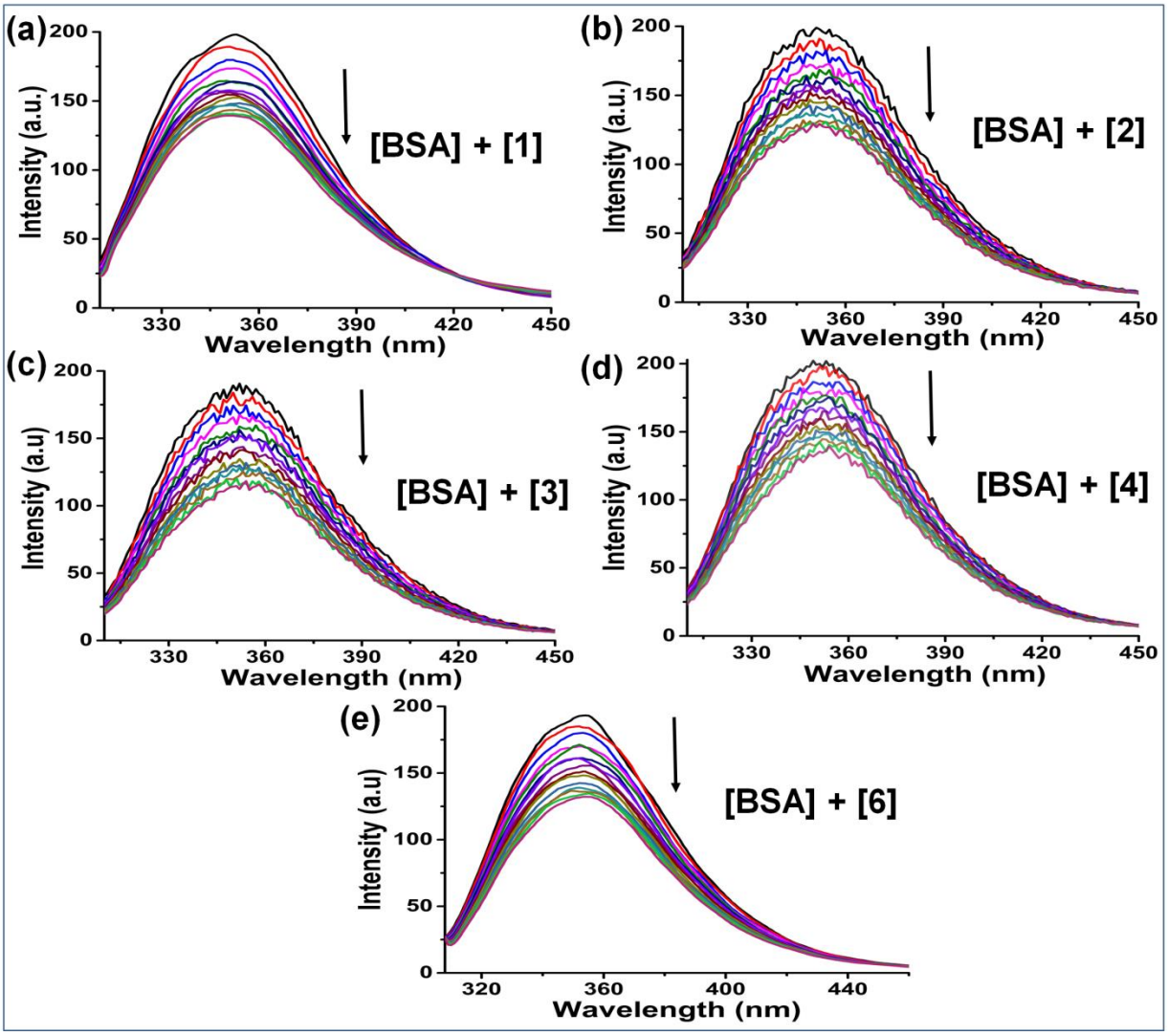

Fig. S36. The BSA (2 μM) binding studies of the complexes (0−3.5 μM) in 0.7% (v/v) DMF−5 mM Tris-HCl/NaCl buffer (pH = 7.2) mixture showing fluorescence emission quenching at 298 K, $\lambda_{exc/em}$ = 295/345 nm and slit width exc/em = 10/5 nm, (a) **1**; (b) **2**; (c) **3**; (d) **4** and (e) **6**.

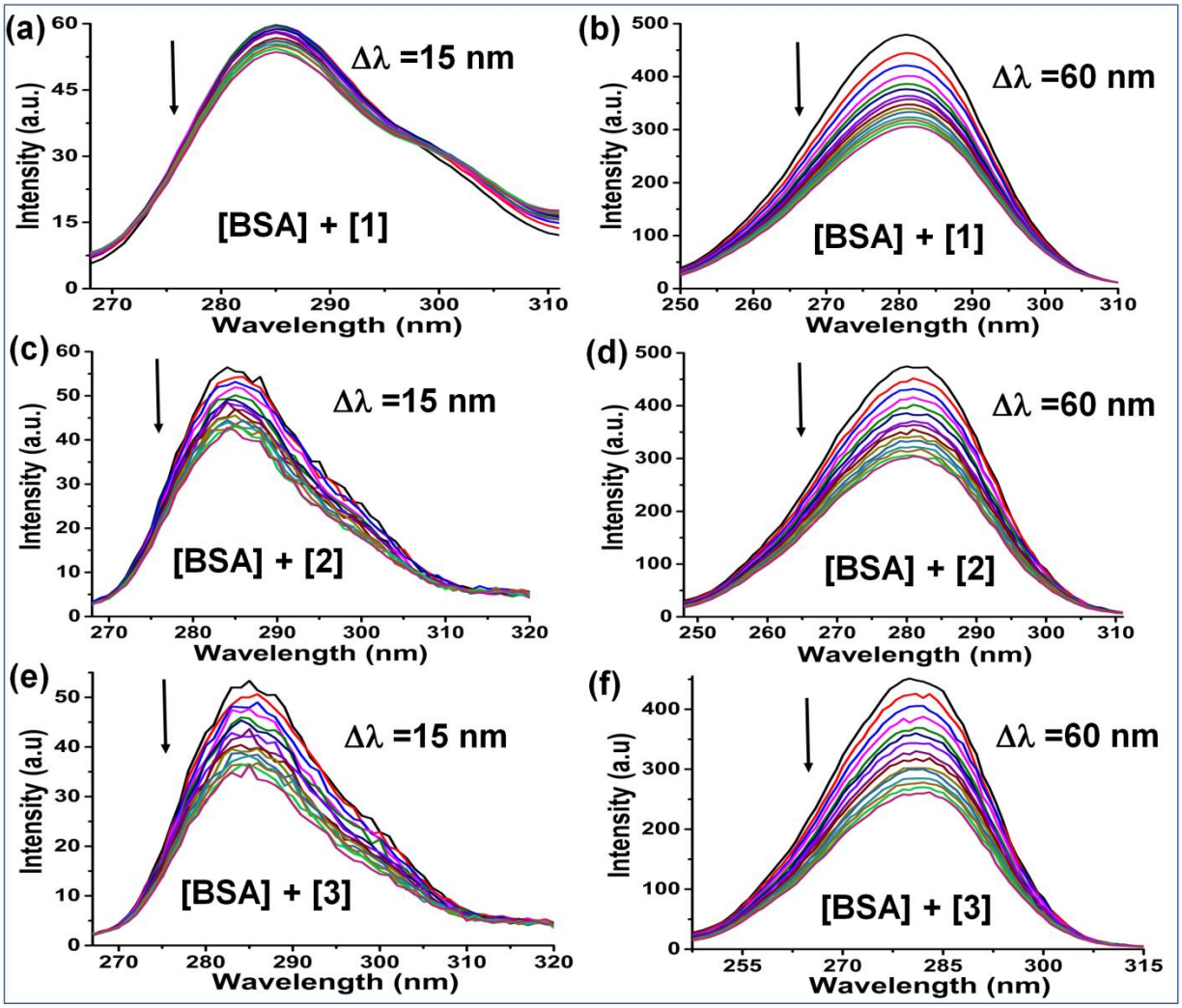

Fig. S37. The synchronous fluorescence spectral traces of the BSA (2 μM) upon addition the complexes (0−3.5 μM) in 0.7% (v/v) DMF−5 mM Tris-HCl/NaCl buffer (pH = 7.2) mixture at 298 K, slit width exc/em = 10/5. (a) Complex **1** with $\Delta\lambda$ = 15 nm and (b) with $\Delta\lambda$ = 60 nm. (c) Complex **2** with $\Delta\lambda$ = 15 nm and (d) with $\Delta\lambda$ = 60 nm. (e) Complex **3** with $\Delta\lambda$ = 15 nm and (f) with $\Delta\lambda$ = 60 nm.

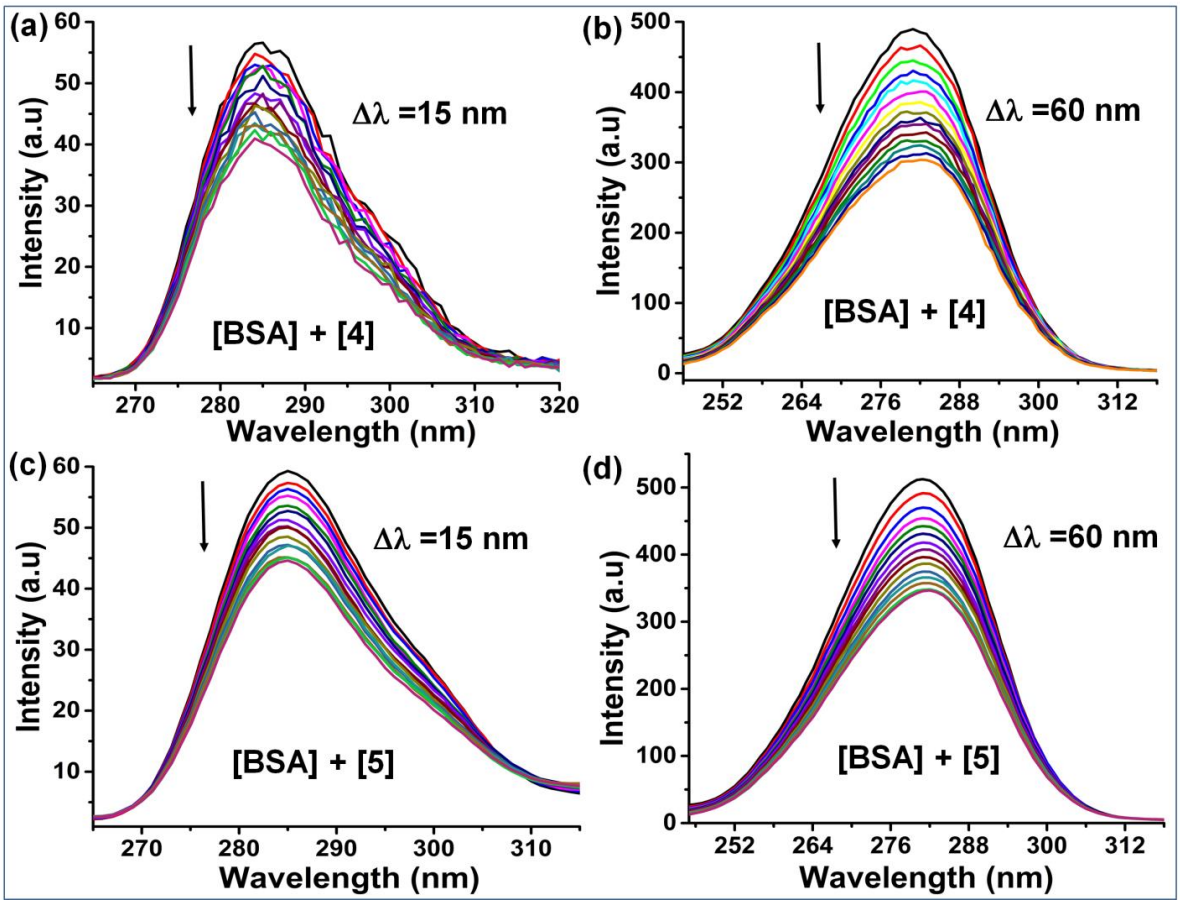

Fig. S38. The synchronous fluorescence spectral traces of the BSA (2 μM) upon addition the complexes (0−3.5 μM) in 0.7% (v/v) DMF−5 mM Tris-HCl/NaCl buffer (pH = 7.2) mixture at 298 K, slit width exc/em = 10/5. (a) Complex **4** with $\Delta\lambda$ = 15 nm and (b) with $\Delta\lambda$ = 60 nm. (c) Complex **5** with $\Delta\lambda$ = 15 nm and (d) with $\Delta\lambda$ = 60 nm.

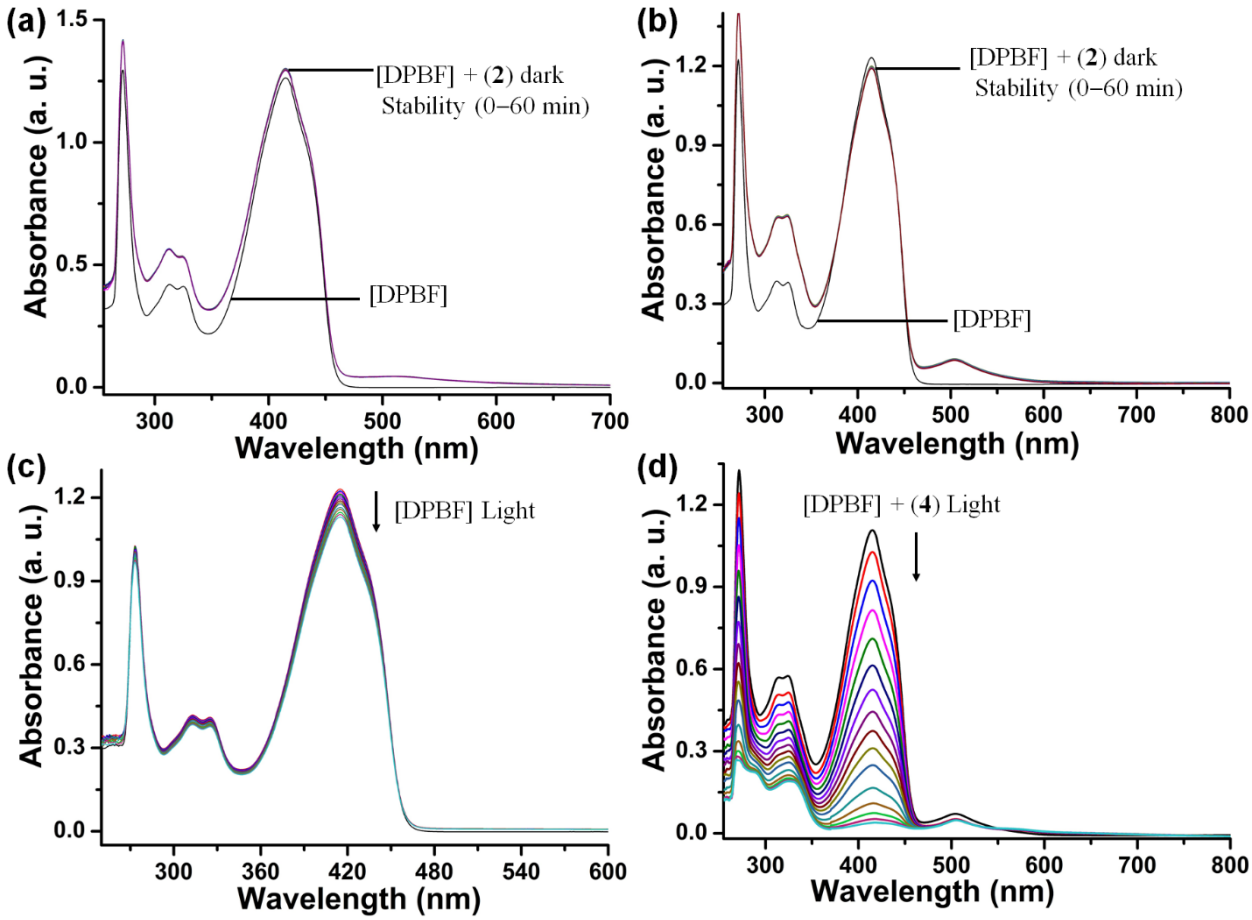

Fig. S39. Absorption spectral profile of (a) DPBF (50 μM) with complex **2** (10 μM) in dark for 0–60 min. (b) DPBF (50 μM) with complex **4** (10 μM) in dark for 0–60 min. (c) DPBF (50 μM) upon photoexposure of green light (530 nm) for 0–600 s. (d) DPBF (50 μM) with **4** (10 μM) upon photoexposure of green light (530 nm) for 0–600 s. Spectra recorded at 298 K in DMF solution.

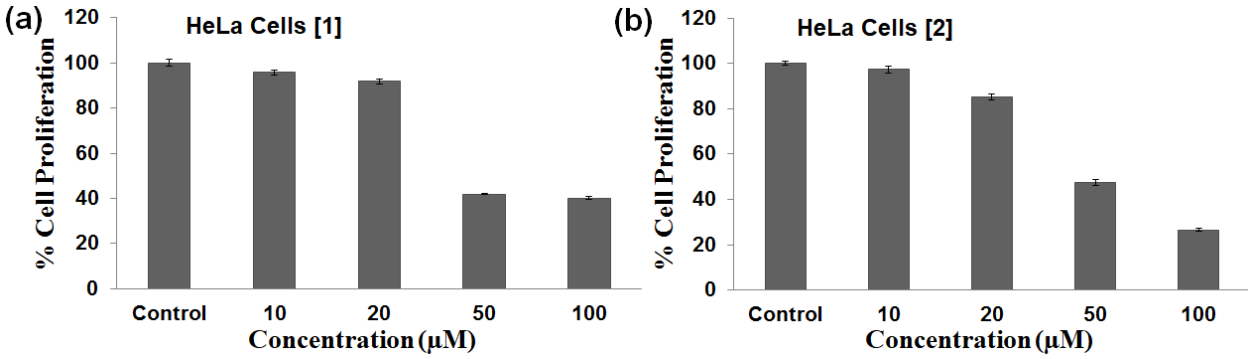

Fig. S40. The dose-dependent cytotoxicity profile of complexes **1** and **2** in dark for HeLa cells from MTT assay determined after 24 h.

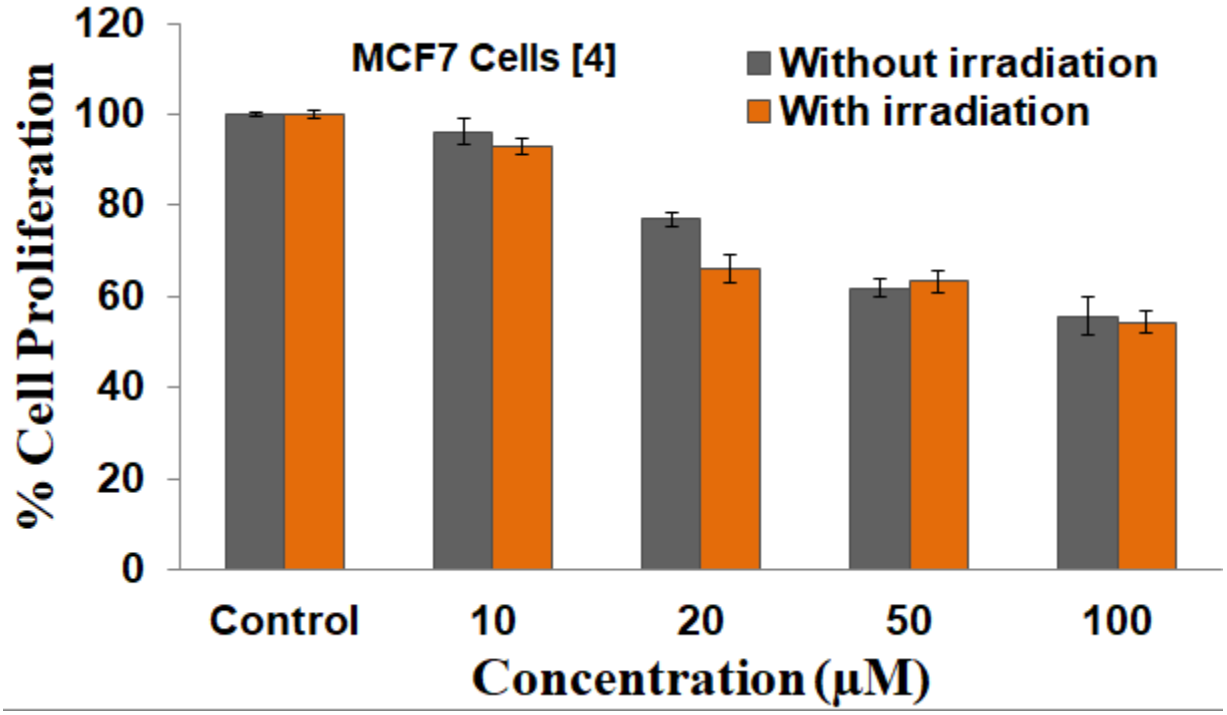

Fig. S41. The comparison of dark and white light (λ_{ex} > 400 nm, 5V, 0.3 W) induced dose-dependent toxicity of the complex [Ru(ttpy)(sac)$_2$(H$_2$O)] (**4**) in MCF7 cancer cells determined from MTT assay. Photoexposure time 1 h followed by incubation for 24 h.

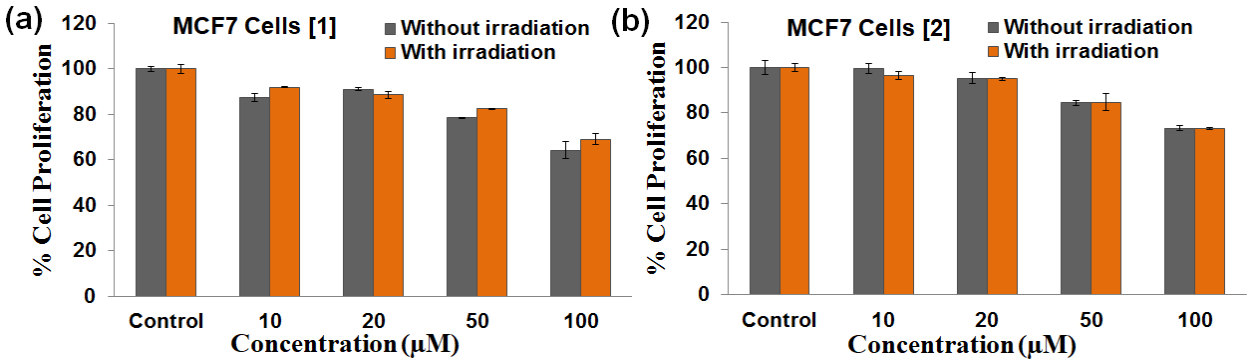

Fig. S42. The comparison of dose-dependent dark and photocytotoxicity induced from UV-A light exposure for 1 h (λ_{ex} = 365 nm, 6 W) of complexes **1** and **2** in MCF7 cancer cells determined from MTT assay.

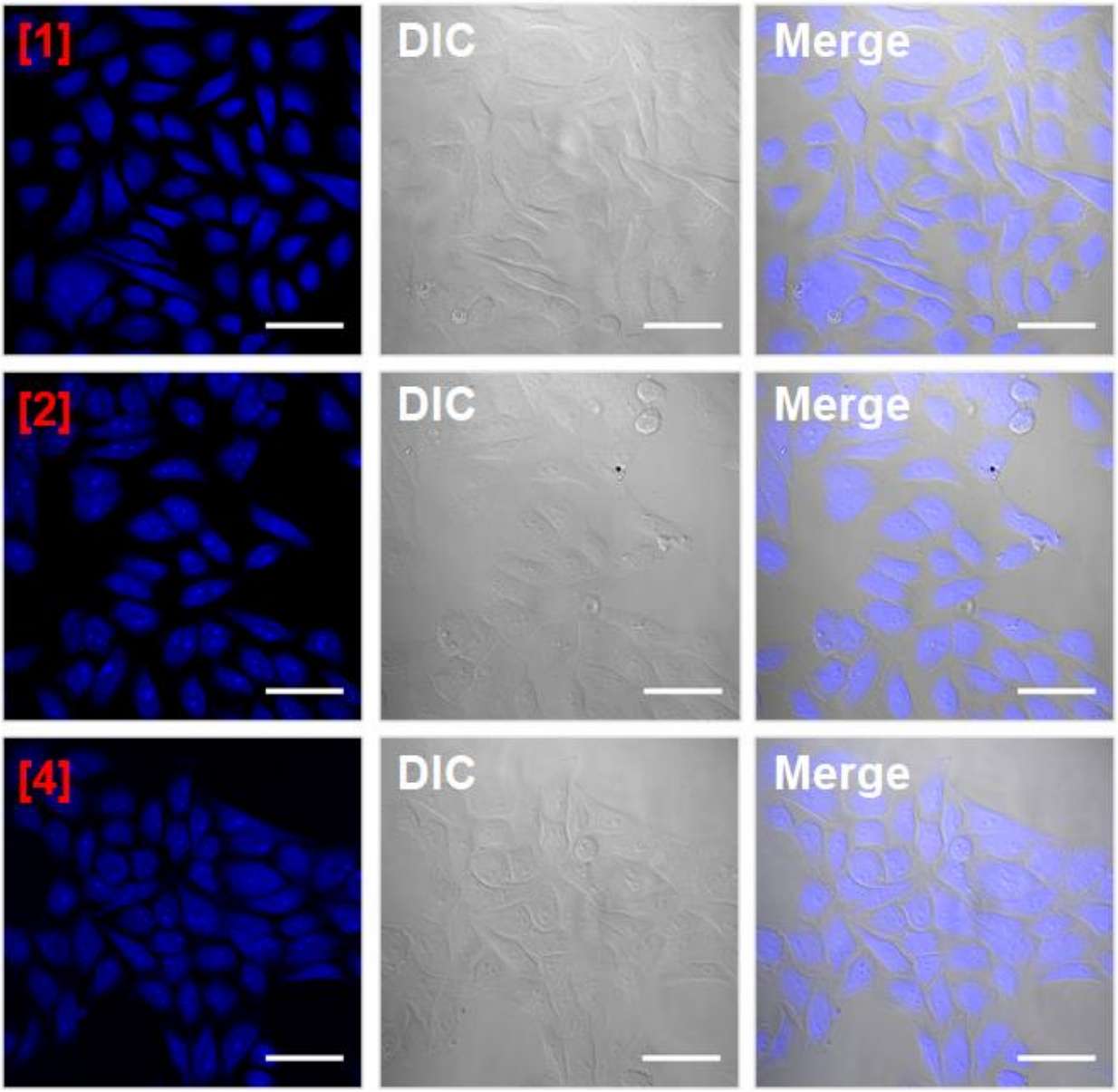

Fig. S43. CLSM images of HeLa cell lines incubated with complexes **1**, **2** and **4** (10 μM) for 4 h. Cells showing blue fluorescence at λ_{ex} = 350 nm and λ_{em} = 460 nm. Merged images demonstrating nucleus and cytosolic localization of complex **1**, **2**, and **4**. Scale bar = 50 μm.

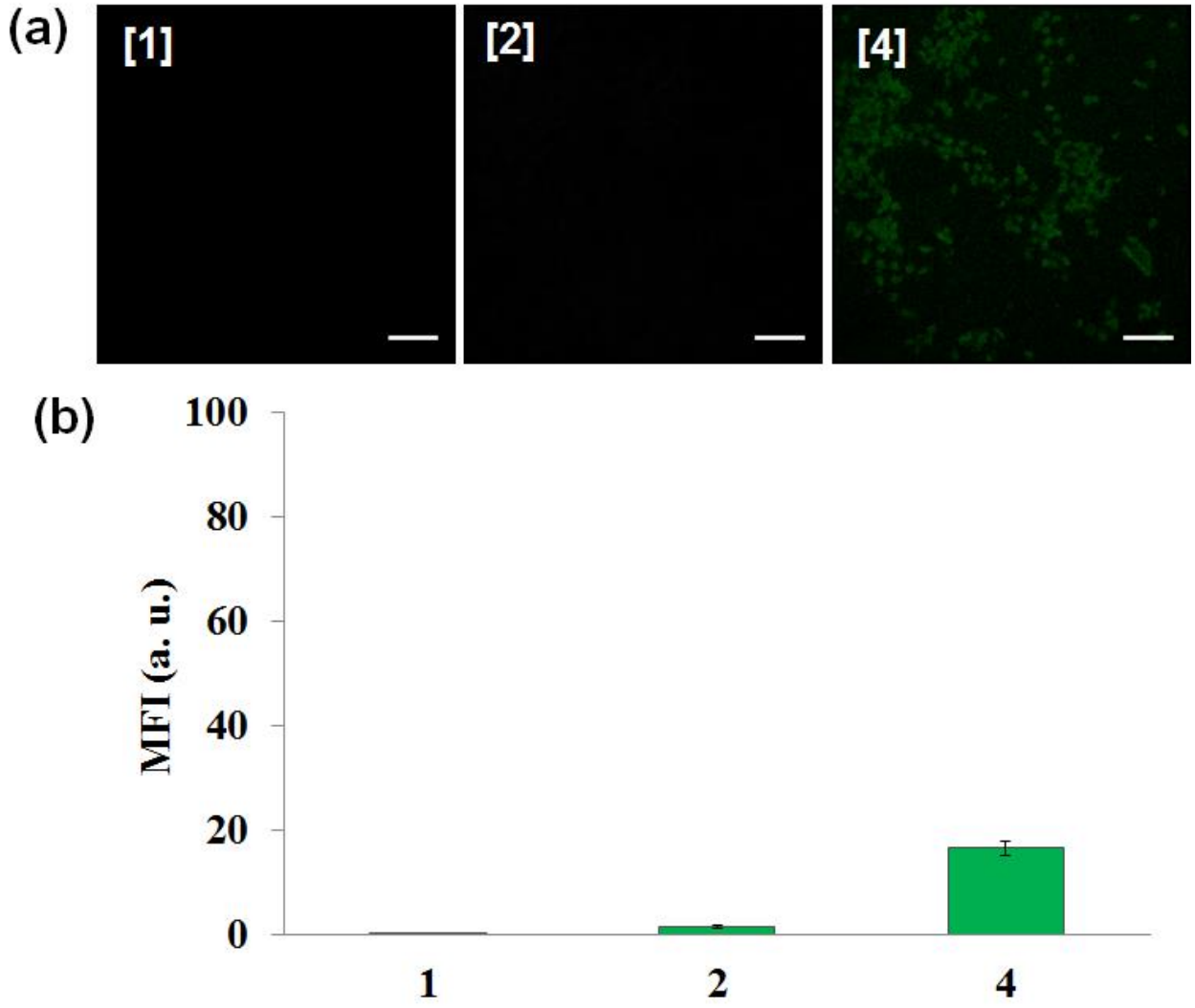

Fig. S44. Detection of intracellular reactive oxygen species (ROS) from H_2DCFDA assay. (a) The confocal laser scanning fluorescence microscopy (CLSM) images of MCF7 cells after 4 h treatment with complexes **1**, **2**, **4** (10 μM) in dark, λ_{ex} = 492 nm, λ_{em} = 527 nm, scale bar = 100 μm. (b) Quantitative analysis comparing the levels of ROS intermediates in untreated and treated MCF7 cells in dark. Values are mean ± S.D from three independent experiments (n = 3).